

C-86 - Nuclear Rocket and Ram-Jet Engines
EXTERNAL TRANSMITTAL AUTHORIZED
Distribution Limited to Recipients Indicated

ORNL

Central Files Number
58-7-4

ORNL

MASTER COPY

75749

ANALYTICAL STUDY OF SOME ASPECTS
OF VORTEX TUBES FOR GAS-PHASE
FISSION HEATING

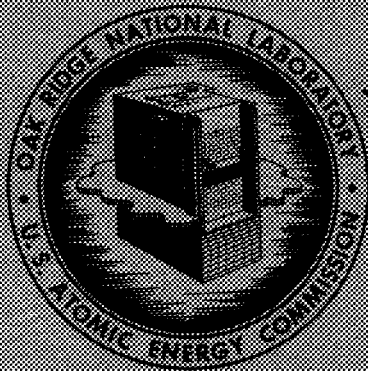
DECLASSIFIED

By Authority of

ACE 9-2-60

JMN

for H. I. Berg, Supervisor
Laboratory Records Dept.
ORNL



NOTICE

This document contains information of a preliminary nature and was prepared primarily for internal use at the Oak Ridge National Laboratory. It is subject to revision or correction and therefore does not represent a final report. The information is not to be abstracted, reprinted or otherwise given public dissemination without the approval of the ORNL patent branch, Legal and Information Control Department.

OAK RIDGE NATIONAL LABORATORY

operated by

UNION CARBIDE CORPORATION

for the

U.S. ATOMIC ENERGY COMMISSION

RELEASE APPROVED
BY PATENT BRANCH

1-17-61 [Signature]
DATE SIGNATURE



C-86 NUCLEAR ROCKET ENGINES

External Transmittal Authorized
Distribution Limited to
Recipients Indicated

ORNL
Central Files Number
58-7-4

This document consists of 84 pages.
Copy 3 of 3 copies. Series ~~A~~

Analytical Study of Some Aspects of
Vortex Tubes for Gas-Phase Fission Heating

J. L. Kerrebrock

P. G. Lafyatis

July 21, 1958

OAK RIDGE NATIONAL LABORATORY
Oak Ridge, Tennessee
operated by
UNION CARBIDE CORPORATION
for the
U.S. ATOMIC ENERGY COMMISSION

Series B
1-3-Lab. Records

Internal Distribution

- | | |
|----------------------|--------------------------|
| 1. F. F. Blankenship | 11. J. L. Kerrebrock |
| 2. E. P. Blizard | 12. J. J. Keys |
| 3. R. A. Charpie | 13. W. D. Manly |
| 4. W. K. Ergen | 14-16. R. V. Meghreblian |
| 5. A. P. Fraas | 17. R. F. Newton |
| 6. J. H. Frye | 18. J. A. Swartout |
| 7. B. L. Greenstreet | 19. A. M. Weinberg |
| 8. W. R. Grimes | 20. E. P. Wigner |
| 9. H. W. Hoffman | |
| 10. W. H. Jordan | |

External Distribution

- 21. A. H. Flagg, Aerojet-General Corp.
- 22. AFPR, Douglas, Long Beach
- 23. AFPR, North American Conoga Park
- 24. AFPR, North American Downey
- 25. Air Research and Development Command (RDGN)
- 26. Air Research and Development Command (RDZPSP)
- 27. Air Technical Intelligence Center
- 28. ANP Project Office, Convair, Fort Worth
- 29. Albuquerque Operations Office
- 30. Armed Forces Special Weapons Project, Sandia
- 31. Armed Forces Special Weapons Project, Washington
- 32. Army Ballistic Missile Agency
- 33. Assistant Secretary of Defense, Rand (WSEG)
- 34.-37. Atomic Energy Commission, Washington
- 38. Bureau of Aeronautics
- 39. C. D. Pengelley, BAR, Glenn L. Martin, Baltimore
- 40. Bureau of Ordnance
- 41. Bureau of Ordnance (SP-209)
- 42. Bureau of Ships
- 43. General Electric Company (ANPD)
- 44. Headquarters, Air Force Special Weapons Center
- 45. J. B. Robinson, III, Headquarters, USAF, Washington
- 46.-47. F. Goddard, Jet Propulsion Laboratory
- 48. H. J. Stewart, Jet Propulsion Laboratory
- 49. P. Wegener, Jet Propulsion Laboratory
- 50.-51. J. Todd, Los Alamos Scientific Laboratory
- 52. Marquardt Aircraft Company
- 53.-54. F. E. Rom, National Advisory Committee for Aeronautics, Cleveland
- 55. National Advisory Committee for Aeronautics, Washington
- 56. Office of Naval Research
- 57. Office of the Chief of Naval Operations (Op-361)
- 58. Office of the Chief of Ordnance
- 59. Patent Branch, Washington
- 60. Redstone Arsenal
- 61. San Francisco Operations Office
- 62.-63. G. Safanov, USAF Project RAND
- 64. U. S. Naval Ordnance Test Station
- 65.-66. University of California Radiation Laboratory, Livermore
- 67.-68. Western Development Division
- 69.-74. Wright Air Development Center (WCCSI-3)
- 75.-109. Technical Information Service Extension, Oak Ridge

Summary

Several problems connected with vortex cavity reactors have been studied analytically. They include; the generation of high strength vortices by utilization of bleed through a porous tube wall to stabilize the shear layer on the wall; the nuclear criticality problem; the suitability of various compounds of plutonium as gaseous fissionable materials; the problem of retaining the fission fragments within the vortex tube.

It is concluded that the shear layer on the vortex tube wall can be stabilized if a mass flow greater than or equal to the vortex through flow is bled through the porous wall, and that the tangential Mach numbers which can be obtained are then slightly more than one half the inviscid values.

Beryllium oxide or graphite moderated reactors of reasonable size and weight can attain criticality if the product of the hydrogen pressure in the vortex core and the maximum value of the ratio of fissionable gas density to hydrogen density in the tube is greater than about 100 atmospheres. The reactor weights are then in the order of 50,000 pounds or less.

Of the several compounds of plutonium considered as gaseous fuel carriers, plutonium trifluoride and plutonium tribromide appear to be the most promising. It is probable that they can be held in gaseous form in hydrogen, under the desired concentrations.

The rate of loss of fission fragments from the vortex tube can be reduced to a small fraction of the rate of their generation by making the vortex tubes about twice the minimum size which is allowable for satisfactory retention of the fissionable material.

Table of Contents

	Page
Summary	3
General Introduction	5
Section I - Vortex Recirculation	7
Influence of wall bleed on the vortex	8
Effectiveness of vortex formation	11
Stabilization of the shear layer	13
Effect of wall bleed on the separation process	17
Recirculation systems	21
Gas turbine cycle	22
Propellant turbine cycle	28
Conclusions	33
Section II - Criticality	35
Derivation of nuclear constants from separation calculations	36
Reactor code	40
Results	41
Conclusions	47
Section III - Gaseous Fissionable Compounds for Vortex Reactors	48
Possible fuel carriers	49
Volatility	50
Chemical equilibrium	50
Calculation of free energies	53
Requirements imposed by vapor pressure and equilibrium	60
Conclusions	60
Section IV - Fission Product Retention	62
Nomenclature	64
Differential equations	66
Boundary conditions	70
Leakage rate	71
Numerical example	72
Conclusions	78
References	81
List of figures	83

INTRODUCTION

A method was proposed in Ref. 1 for holding gaseous fissionable material in a vortex tube, against the radial flow of a fluid which was to be heated to a high temperature. The process of diffusion of a low molecular weight gas through the high molecular weight fissioning gas was considered in some detail. It was concluded that if laminar vortices of the required strength could be generated with the radial mass flow rates required by the diffusion process, then the vortex tube held promise as a device for producing very high temperature gases, for example for rocket propulsion.

In the first section of this report, a method for producing laminar vortices of the required strength will be suggested. It consists of a recirculatory system in which the mass flow through the tangential vortex-driving nozzles is increased beyond the amount allowed by the radial diffusion process; the excess mass flow is bled off through a porous vortex tube wall. The bled fluid must be returned to the nozzle entrance conditions, and some methods for doing this will be proposed. Bleeding of the fluid through the porous wall is equivalent to sucking a boundary layer; the shear layer on the vortex tube wall is thinned and its Reynolds' number reduced. Thus, there seems to be some possibility that the shear layer may be stabilized and a laminar vortex produced. The scheme has the additional advantage that the porous tube wall will be effectively cooled by the bled fluid.

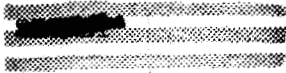
Although the diffusion-heating process considered in Ref. 1 is evidently the key problem to be solved in applying the vortex tube to rocket propulsion, the high temperatures envisioned, and the gaseous state of the fissionable material, give rise to other problems which must be studied before the application of the vortex tube to rocket propulsion can be seriously considered. Some of these problems will be indicated, and the progress made to date in studying them will be summarized.

Because of the gaseous form of the fissionable material, and the limitations imposed by the vortex-separation process⁽¹⁾, it seems that

the fuel concentration in a reactor composed of vortex tubes must be rather low. The available fuel concentrations are about one tenth of the usual values for small, highly poisoned reactors. The critical sizes (and weights) of the vortex reactors thus tend to be large. A series of criticality calculations has therefore been done, with the emphasis on minimizing the reactor weight for a given fuel concentration. These calculations have been carried out by P. G. Lafyatis, and will be discussed in section II.

It was implicitly assumed in Ref. 1 that some compound of plutonium, or uranium, could be found, which could be held in gaseous form under the desired conditions. Rather high concentrations of fissionable material must be held at very high temperatures and under reducing conditions, if hydrogen is to be used as propellant. There is some doubt as to whether any material can be found which will satisfy these requirements, since the compounds of uranium and plutonium which are stable at high temperatures are neither very volatile nor very resistant to reduction by hydrogen. This problem will be considered in section III.

The fissioning of uranium or plutonium in the vortex tubes will produce rather large quantities of very radioactive fission products. If these fission products are discharged to the atmosphere contamination will result. However, since the fission products will in general have rather high molecular weights, there is some possibility that a considerable fraction of those produced will be held in the vortex tubes along with the fissionable material. A calculation of the rate of loss of the fission fragments from the vortex tube has been carried out by the methods used in Ref. 1, and will be discussed in section IV.



SECTION I

Vortex Recirculation



Introduction:

In the analysis of vortex heating-separation tubes presented in Ref. 1, it was assumed that the flow in the vortex tube was laminar and inviscid. It was demonstrated that, for laminar flow, viscous effects would not prevent the formation of vortices of sufficient strength to give the desired separation. It was also pointed out that even though the Reynolds' number (based on tube diameter and tangential velocity) of the flow is very large, there is a possibility of obtaining laminar flow because of the large density gradients produced by the action of the vortex field on the heavy fissionable gas. However, if this stabilizing effect is not sufficient to maintain laminar flow, there seems to be little possibility of obtaining vortices of adequate strength in the simple tube described in Ref. 1.

Accordingly, a method of improving the effectiveness of vortex formation has been considered. The essential idea is to reduce the Reynolds' number of the wall shear layer, by bleeding fluid through a porous wall, to the extent that it will remain laminar. The viscous effects on the vortex strength will then be predictable, and much smaller than they would be if the shear layer were turbulent.

All of the fluid which is bled from the vortex tube through its porous wall must be returned to the conditions at the entrance to the inlet nozzles, and recycled, at least for rocket propulsion applications. It seems possible to do this by means of a gas turbine cycle operating between the reactor as a heat source and the fresh propellant as a heat sink.

It is logical to divide the following discussion into two parts. In the first, the influence of the porous wall bleed on the velocity profile, vortex strength, and radial diffusion, is considered. In the second, some methods of recycling the bled fluid are discussed.

Influence of wall bleed on the vortex:

It was shown in Ref. 1 that the tangential momentum equation for the vortex flow may be written as follows, if the flow is laminar:

$$\frac{d(v_o/v_j)}{dr'} + \frac{(v_o/v_j)}{r'} = - \frac{2\pi\mu}{\eta} r' \left\{ \frac{d^2(v_o/v_j)}{dr'^2} + \frac{1}{r'} \frac{d(v_o/v_j)}{dr'} - \frac{(v_o/v_j)}{r'^2} \right\} \quad I-(1)$$

SECRET

The tangential velocity, v_o , is referred to the exit velocity from the inlet nozzles, v_j , and the radius has been made dimensionless by division by the radius at which the jets enter the tube (see Fig. 1). \dot{m} is the radial mass flow rate, and is positive for inward flow. It has been assumed in writing Eq. (1) that μ is constant. Inclusion of the variation of μ would complicate the following analysis greatly, and would not change the results significantly.

From Eq. (1), it is clear that the quantity $2\pi\mu/\dot{m}$, which will be denoted by K , measures the importance of viscous effects in the vortex. If the absolute value of K is large, viscous forces predominate; if it is small, inertial forces predominate. The solution of Eq. (1) may be written as

$$\frac{v_o}{v_j} = A_1(r')^{-\frac{1-K}{K}} + A_2(r')^{-1} . \quad I-(2)$$

The flow consists of two regions. In the inner region ($r' < 1$), K is positive, while in the outer region ($r' > 1$), K is negative. Appropriate boundary conditions are as follows:

1. The velocity must be continuous at $r' = 1$.
2. The torque exerted on the exterior region by the interior region, at $r' = 1$, must be zero.
3. The velocity must be zero at the tube wall.
4. The torque exerted on the fluid in the tube, by the entering jets of fluid, must equal that due to viscous shear at the tube wall.

The last two conditions are sufficient to specify the flow in the outer region, since the last condition effectively determines v_o at $r' = 1$. The first two conditions would then determine the flow in the inner region, but this information will not be needed in the following analysis. Applying the third boundary condition we find,

UNCLASSIFIED
ORNL-LR-DWG 31874

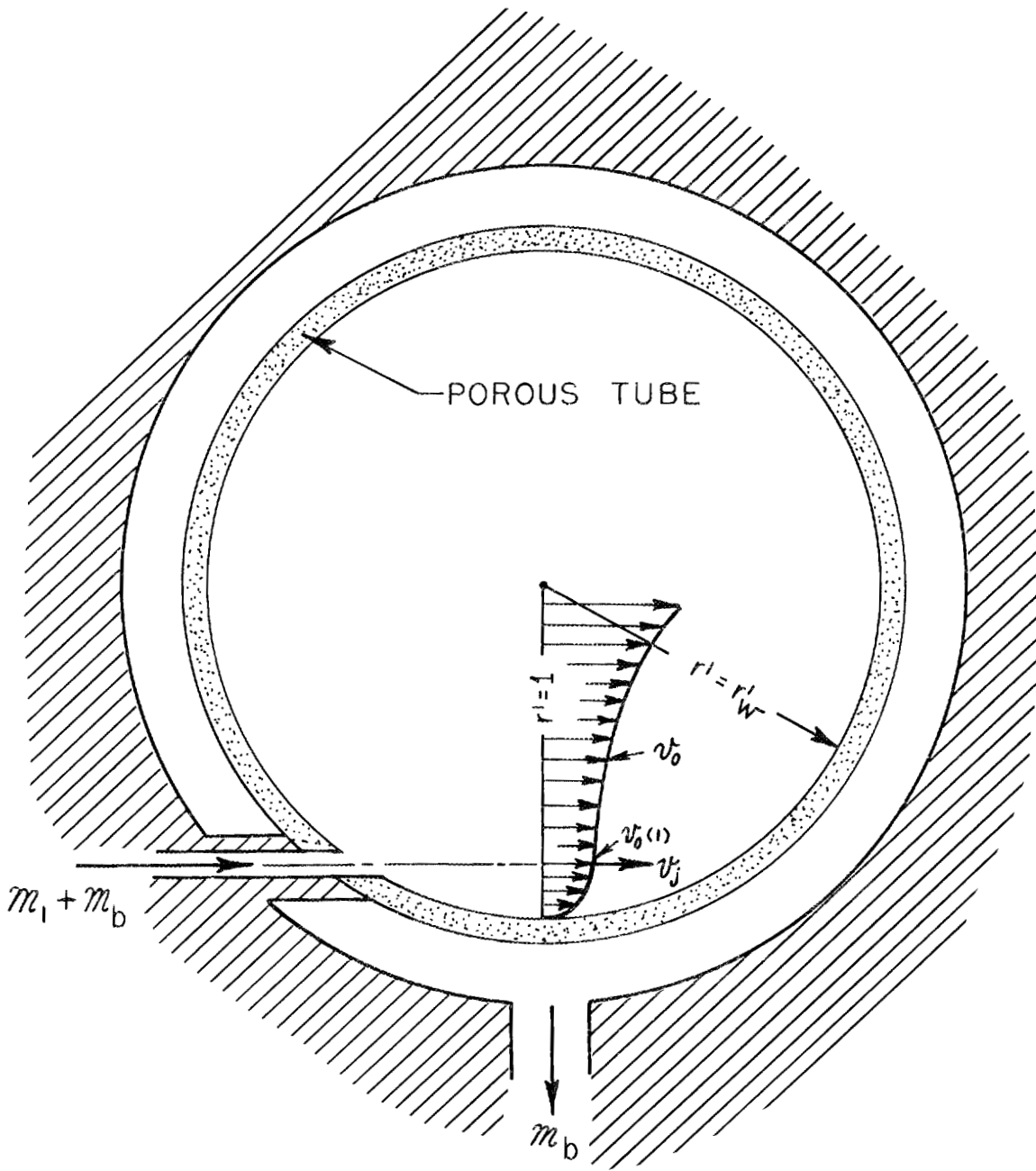


Fig.1. Withdrawal of fluid through Porous Wall.

$$A_2 = -A_1(r'_w)^2 - \frac{1}{K},$$

where r'_w is the value of r' corresponding to the tube radius. The fourth condition gives

$$(\mathcal{M}_1 - \mathcal{M}_b) \left[1 - \frac{v_o(1)}{v_j} \right] = -\mu \frac{d}{dr'} \left(\frac{v_o}{v_j} \right) \Big|_{r'_w} 2\mathcal{M}(r'_w)^2,$$

where \mathcal{M}_1 and \mathcal{M}_b are the radial and bled mass flows.

We then have,

$$\frac{v_o}{v_o(1)} = (r')^{-1} \left\{ \frac{(r')^2 - \frac{1}{K} - (r'_w)^2 - \frac{1}{K}}{1 - (r'_w)^2 - \frac{1}{K}} \right\} \quad \text{I-(3)}$$

where

$$\frac{v_o(1)}{v_j} = \frac{1}{1 + \frac{1 - 2K}{\left(1 - \frac{\mathcal{M}_1}{\mathcal{M}_b}\right) \left[1 - (r'_w)^{\frac{1}{K} - 2}\right]}} \quad \text{I-(4)}$$

Effectiveness of vortex formation:

The effectiveness of vortex formation is indicated directly by the ratio $v_o(1)/v_j$, from Eq. (4). This ratio is plotted in Fig. 2, for a range of $\mathcal{M}_b/\mathcal{M}_1$, for $2\mu/\mathcal{M}_1 = 0.02$. The values indicated in Fig. 2 for $\mathcal{M}_b/\mathcal{M}_1 = 0$ are somewhat smaller than were given in Ref. 1, Fig. 23.

UNCLASSIFIED
ORNL-LR-DWG 30565

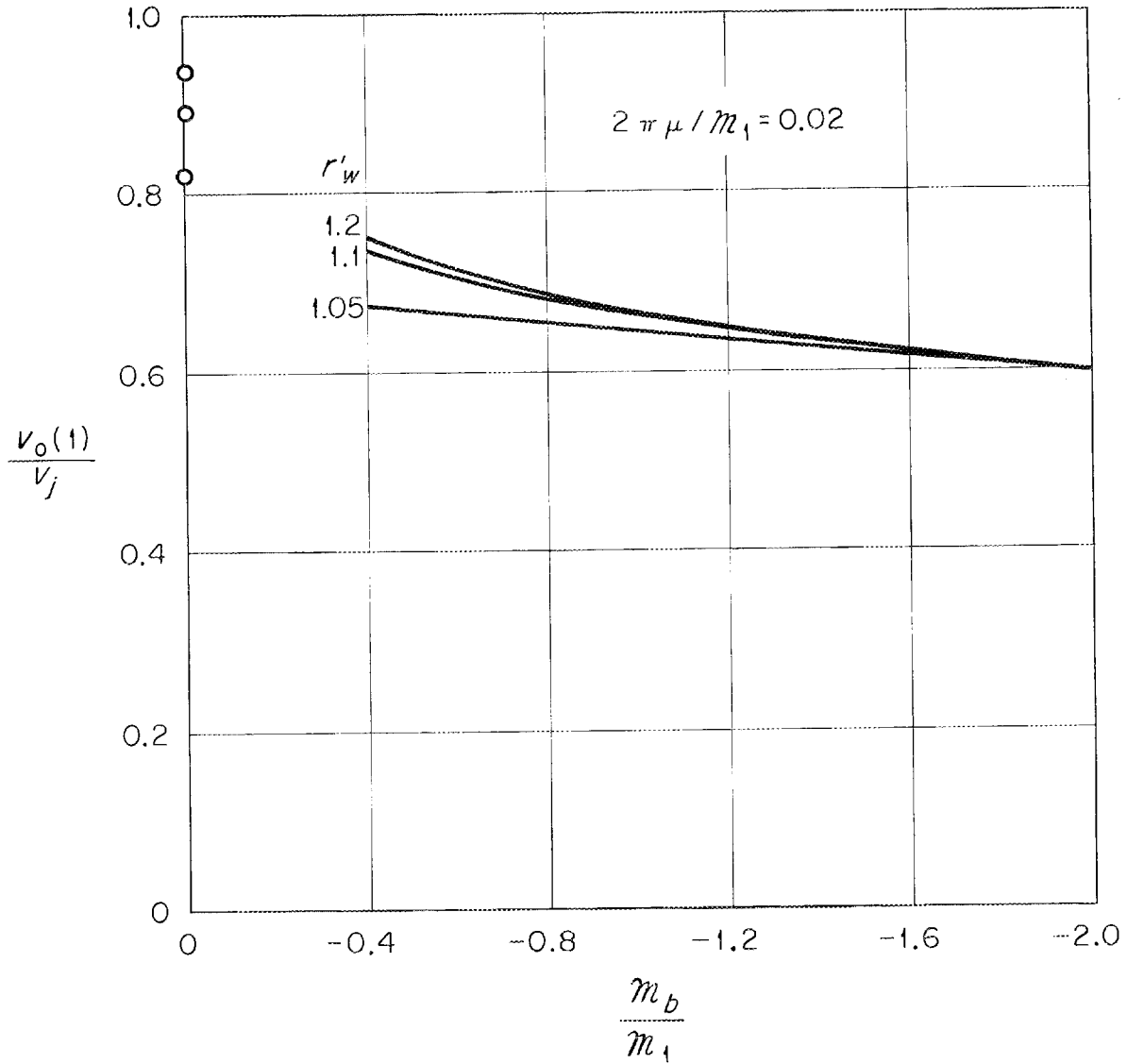


Fig. 2. Variation of Effectiveness of Vortex Formation, $v_0(1)/v_j$, with Bleed to Radial Mass Flow Ratio, m_b/m_1 , and Dimensionless Tube Radius r_w .

A factor of two was omitted from the second term in the denominator of Eq. (55) of Ref. 1.

It is clear that bleeding through the wall reduces the strength of a laminar vortex, but not to a very large extent. As $K \rightarrow 0$ for fixed M_1 , Eq. (4) gives $v_o(1)/v_j = 1/2$ as a limiting value. Thus, if the vortex can be kept laminar by bleeding through a porous wall, it seems that tangential velocities greater than one half the inviscid values will be obtained.

Stabilization of the shear layer:

Calculations of the stability of laminar shear flows result in curves giving the Reynolds' number for which the shear layer is neutrally stable to excitation of a specified wave length. For each such curve there is some Reynolds' number below which the shear layer is stable to excitation of all wave lengths. This value is usually termed the critical Reynolds' number, Re_{cr} .

The critical Reynolds number is defined in terms of the stream velocity at infinity and the displacement thickness of the shear layer. Its value depends rather strongly on the velocity profile in the shear layer, ranging from about 420 for a Blasius profile on a flat plate to 70,000 for an asymptotic suction profile on a flat plate⁽²⁾.

For the shear layer on the vortex tube wall we may define a displacement thickness, δ^* , by:

$$\delta^* = r_w \int_1^{r'_w} \left\{ 1 - \frac{v_o}{v_o(1)} \right\} dr' \tag{I-5}$$

Using Eq. (3), we find:

$$\frac{\delta^*}{r_w} = \frac{r'_w - 1 - \frac{1}{3 - \frac{1}{K}} \left[(r'_w)^3 - \frac{1}{K} - 1 \right]}{1 - (r'_w)^2 - \frac{1}{K}} \tag{I-6}$$

Now the velocity ratio, $v_o/v_o(1)$ may be given as a function of $(r_w - r)/\delta^* = (r'_w - r')r_w/\delta^*$. A typical vortex tube shear layer profile is compared to the Blasius and asymptotic suction profiles in this fashion in Fig. 3. It appears that the vortex tube profile is very close to the plate suction profile, apart from a scale factor which results from the finite limit in the above definition of δ^* . Thus, if the density were constant through the shear layer, its critical Reynolds' number would be slightly greater than 0.7×10^5 . It will be shown in the next section that the influence of the wall bleed on the heavy gas is such as to produce an appreciable positive density gradient in the direction of increasing r' . Such a density gradient, in combination with the radial force field produced by the vortex, will tend to stabilize the shear layer, hence it is concluded that the critical Reynolds' number will be somewhat greater than 10^5 .

Ratios of δ^* to the tube radius, computed from Eq. (6), are shown in Fig. 4. It is clear that bleeding reduces the displacement thickness markedly, for fixed r'_w . In fact, for K sufficiently small, and r'_w not too near unity, δ^*/r_w is very nearly equal to $-K r'_w$.

The significance of the above values will be best illustrated by an example. From Table I, p. 61, Ref. 1, the Reynolds' number for case 2 is found to be: $Re = 7.38 \times 10^6 (\delta^*/r_w)$, for a tube radius of one inch. Thus, we find the following values:

m_0/m_1	-0.17	-0.33	-0.67	-1.35	-6.7
K	-0.04	-0.02	-0.01	-0.005	-0.001
Re	2.0×10^5	1.4×10^5	0.96×10^5	0.38×10^5	0.74×10^4

If the above estimate of 10^5 for Re_{cr} is valid, the shear layer should be stabilized by a mass flow ratio (bleed to radial) of about unity.

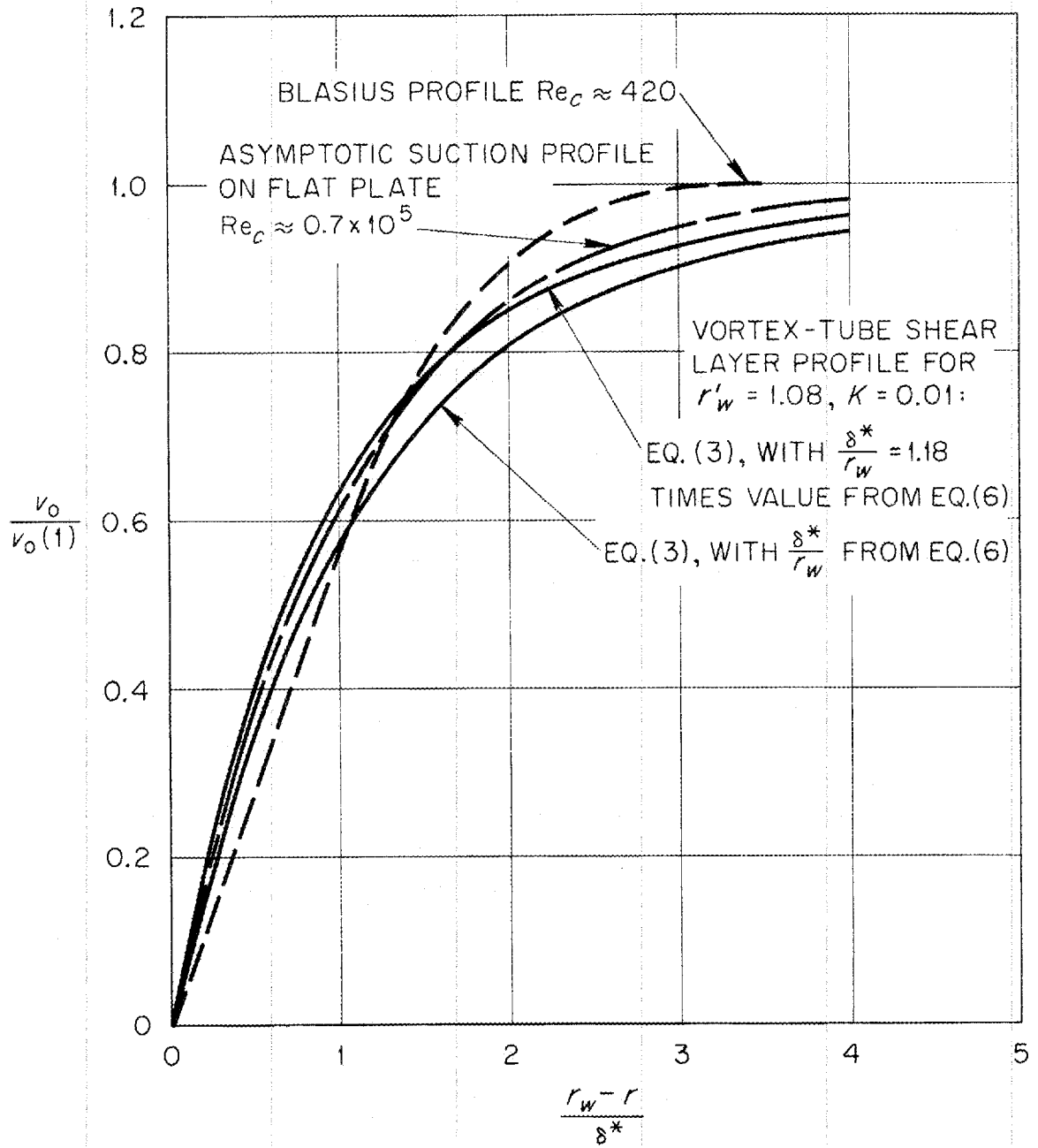


Fig. 3. Comparison of Vortex Tube Shear Layer Velocity Profile with Blasius and Asymptotic Flat Plate Suction Profiles.



UNCLASSIFIED
ORNL-LR-DWG 30567

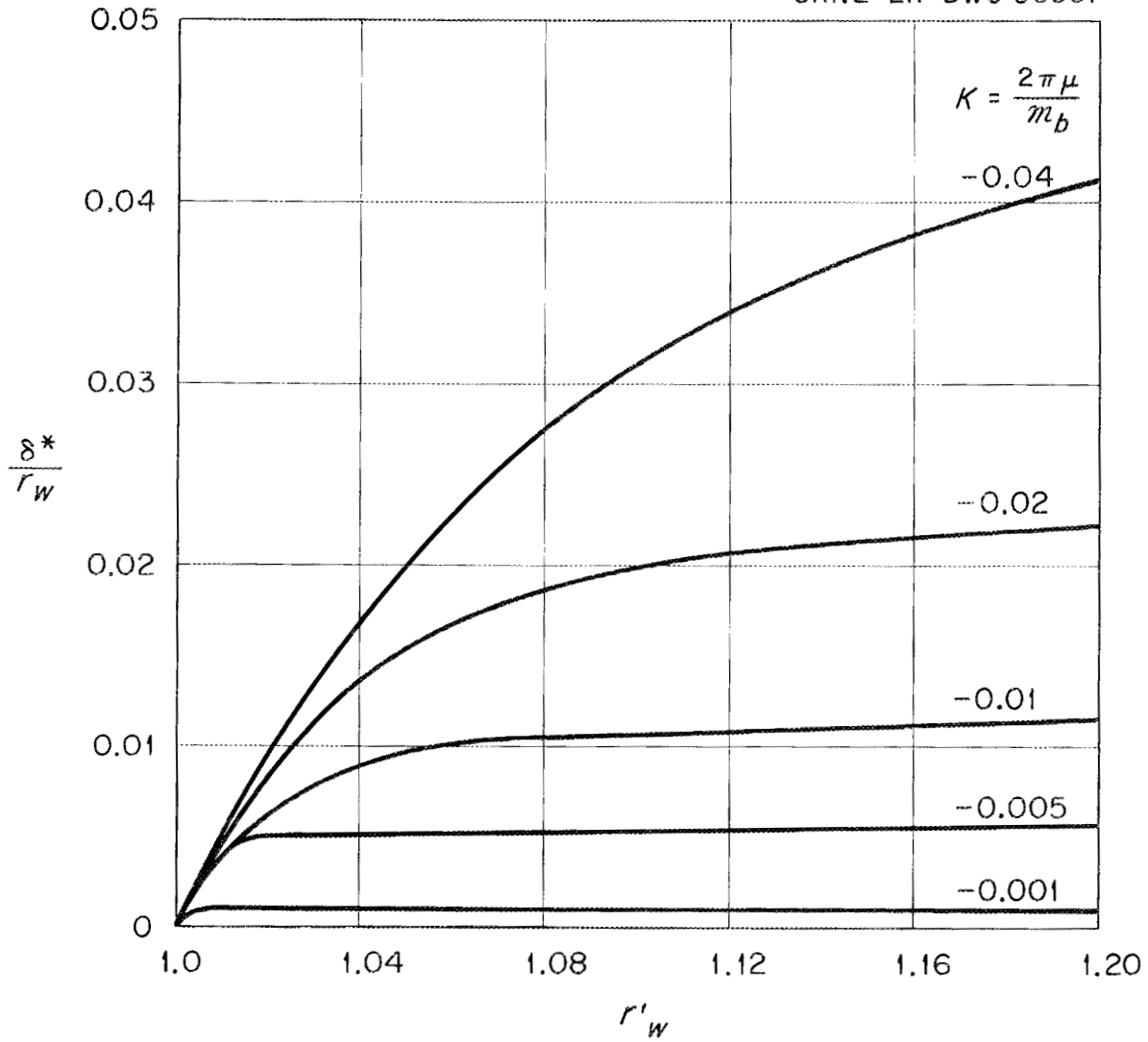


Fig. 4. Variation of Ratio of Shear Layer Displacement Thickness to Tube Radius, δ^*/r_w with Bleed Mass Flow Rate and Dimensionless Tube Radius.

Effect of wall bleed on the separation process:

The analysis of Ref. 1 considered a free vortex with radial flow, bounded on the outside by a solid tube wall. It is now proposed that a region with radial outflow be interposed between the free vortex core and the tube wall. The influence of this region of reversed mass flow on the separation effect will be estimated in this section, by the methods of Ref. 1.

A model for the flow is shown in Fig. 5. It is assumed that fluid is introduced with an effective tangential Mach number M_{tp} , of total amount $\mathcal{M}_1(1 + w_c) - \mathcal{M}_b(1 + w_b)$ per unit of tube length, uniformly over the cylindrical surface of radius $r' = 1$. Of this total amount, $\mathcal{M}_1(1 + w_c)$ then flows inward, while $-\mathcal{M}_b(1 + w_b)$ flows outward. The mass flows of light gas are \mathcal{M}_1 and \mathcal{M}_b , while w_c and w_b are the ratios of heavy gas density to light gas density at the vortex exit and in the gas bled through the wall.

It is readily seen from Eq. (22a) of Ref. 1 that the ratio of heavy gas density to light gas density, w , is governed by the following equation:

$$1 - \frac{w_b}{w} = \mathcal{D}_p \frac{1 + w_b}{1 + w_p} T'^{\frac{1}{2}} \left\{ \left(\frac{m_2}{m_1} - 1 \right) \frac{\gamma M_{tp}^2}{T'} v_o'^2 - \frac{r'}{w} \frac{dw}{dr'} \right\}, \quad I-(7)$$

where the primes indicate values divided by their respective values at $r = r_p$, the jet entry radius. The quantity \mathcal{D}_p is given by Eq. (24) of Ref. 1 as,

$$\mathcal{D}_p = \frac{3(2\pi)^{\frac{1}{2}}}{8} \left(\frac{k^{\frac{1}{2}} m_1^{\frac{3}{2}}}{d_{12}^2} \right) \left(1 + \frac{m_1}{m_2} \right)^{\frac{1}{2}} \left(\frac{1 + w_p}{1 + w_b} \right) \frac{T_p^{\frac{1}{2}}}{\mathcal{M}_b}, \quad I-(8)$$

where k is Boltzmann's constant, d_{12} is the equivalent hard sphere diameter for collisions between light and heavy gas molecules, and m_1 and m_2 are the masses of the light and heavy molecules. M_{tp} is the actual tangential Mach number of the vortex at the jet entry radius.

UNCLASSIFIED
ORNL-LR-DWG 31875

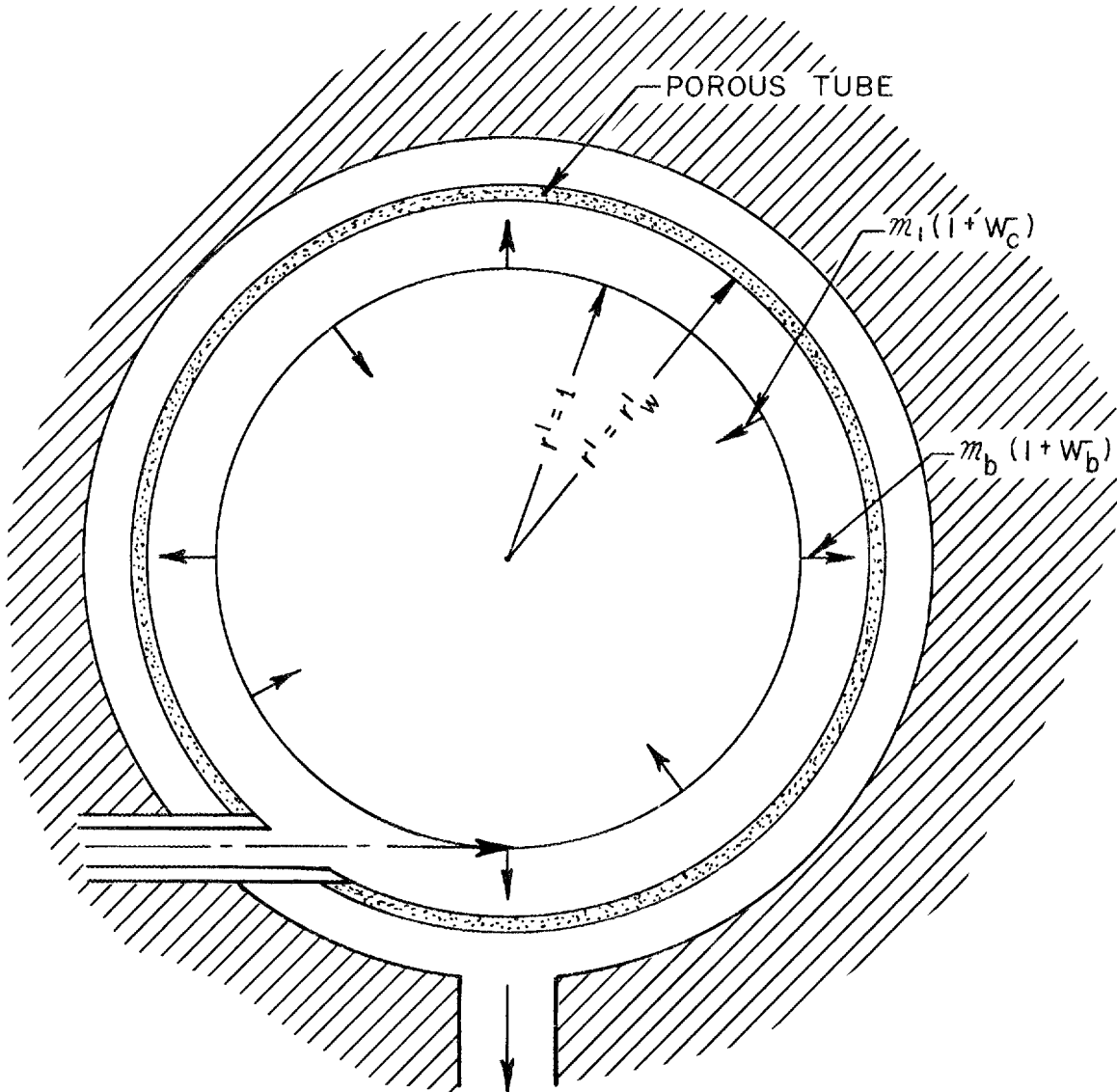


Fig. 5. Model Used for Calculation of Effect of Wall Bleed on Vortex Diffusion.

We wish to investigate the behavior of w in a range of r' from unity to a value, r'_w , slightly greater than unity. Because of the narrow range of r' to be considered, and the fact that T' varies quite slowly with r' in regions of the tube where w is small, T' will be taken equal to unity. It is felt that it will be necessary to insist that w be small near the tube wall if the bleed system is to be used, since otherwise large concentrations of fissionable material would enter the recirculation system. The dimensionless velocity v'_0 , is given by Eq. (3), so that for $T' = 1$, we have,

$$1 - \frac{w_b}{w} = \mathcal{D}_p \frac{1 + w_b}{1 + w_p} \left\{ \frac{m_2}{m_1} - 1 \right\} \gamma M_{tp}^2 \frac{1}{r'^2} \left[\frac{(r')^2 - \frac{1}{K} - (r'_w)^2 - \frac{1}{K}}{1 - (r'_w)^2 - \frac{1}{K}} \right]^2 - \frac{r'}{w} \frac{dw}{dr'} \quad I-(9)$$

The quantity \mathcal{D}_p shows the influence of the radial mass flow on the system. It can be written in terms of the characteristic parameters of the vortex core and the mass flow ratio, m_b/m_1 , as follows (see Eqs. (25) and (34), Ref. 1)

$$\mathcal{D}_p \frac{1 + w_b}{1 + w_p} = T_p^{*2} \frac{1 - w_c/w_m}{\gamma M_{tm}^2 \left(\frac{m_2}{m_1} - 1 \right)} \frac{m_1}{m_b} \quad I-(10)$$

Equation (9) may now be written in the following form:

$$\frac{d \left(\frac{w}{w_b} \right)}{dr'} = \frac{\gamma M_{tm}^2 \left(\frac{m_2}{m_1} - 1 \right)}{\left(1 - \frac{w_c}{w_m} \right) T_p^{*2}} \frac{m_b}{m_1} \left(\frac{1 - \frac{w}{w_b}}{r'} \right) + \gamma M_{tp}^2 \left(\frac{m_2}{m_1} - 1 \right) \left[\frac{(r')^2 - \frac{1}{K} - (r'_w)^2 - \frac{1}{K}}{1 - (r'_w)^2 - \frac{1}{K}} \right]^2 \frac{\left(\frac{w}{w_b} \right)}{r'^3} \quad I-(11)$$

This equation is linear, and hence integrable; however, the general solution is quite involved because the coefficient of w/w_b is complicated. On the other hand, it is expected that w/w_b will be close to unity in the cases of interest. In this case w/w_b may be taken as unity in the last term, to a first approximation. The integration is then easy and yields,

$$1 - \frac{w}{w_b} = \frac{\gamma M_{tp}^2 \left(\frac{m_2}{m_1} - 1 \right) r_w'^2 - \frac{2}{K}}{\left(1 - r_w'^2 - \frac{1}{K} \right)^2} \left\{ \frac{1}{\alpha + 2 - \frac{2}{K}} \left[\left(\frac{r'}{r_w'} \right)^{-\alpha} - \left(\frac{r'}{r_w'} \right)^2 - \frac{2}{K} \right] - \frac{2}{\alpha - \frac{1}{K}} \left[\left(\frac{r'}{r_w'} \right)^{-\alpha} - \left(\frac{r'}{r_w'} \right)^{-\frac{1}{K}} \right] + \frac{1}{\alpha + 2} \left[\left(\frac{r'}{r_w'} \right)^{-\alpha} - \left(\frac{r'}{r_w'} \right)^{-2} \right] \right\} \quad I-(12)$$

where

$$\alpha = \frac{\gamma M_{tm}^2 \left(\frac{m_2}{m_1} - 1 \right) \frac{m_b}{m_1}}{\left(1 - \frac{w_c}{w_m} \right) T_p^{*1/2}}$$

According to the estimates given in the previous sections, K must be of order - 0.01 if the shear layer is to be stabilized, and this gives $m_b/m_1 = - 0.67$, for the example quoted previously. Thus, for the cases considered in Ref. 1, α is about - 100. Since - α and - $1/K$ are then large positive numbers, all terms of Eq. (12) except the last are negligible for r' appreciably less than r_w' . We therefore find,

$$1 - \frac{w}{w_b} \approx \left(1 - \frac{w_c}{w_m} \right) \left(\frac{M_{tp}}{M_{tm}} \right)^2 T_p^{*1/2} \frac{1}{r_w'^2} \left(- \frac{m_1}{m_b} \right). \quad I-(13)$$

For the cases of interest (e.g. case 2, Table I, p. 61, Ref. 1), the factor $(M_{tp}/M_{tm})^{2r^{*1/2}}$ is about unity. Thus at $r^* = 1$, w/w_b is nearly equal to $1 + \dot{m}_1/\dot{m}_b$. If \dot{m}_b/\dot{m}_1 is 2, w_b/w_p is then about 1.5. Replacing w/w_b by unity in the last term of Eq. (17) results in an overestimate of w_b/w_p , since the last term is positive and would in fact be everywhere smaller than it has been assumed to be.

The analysis therefore indicates that the ratio of the wall density ratio to that at the free vortex periphery will be less than 2, if \dot{m}_b/\dot{m}_1 is 2 or more. A mass flow ratio of 2 should, according to the previous section, be sufficient to stabilize the shear layer, so that it seems sufficient to produce the desired vortex strength. Therefore in the following analysis of recirculation systems, a mass flow ratio of 2 will be regarded as a minimum which the recirculation system must allow to be satisfactory.

Recirculation systems:

The purpose of the recirculation system is to return the fluid bled through the porous tube wall to a condition such that it can be reintroduced to the vortices through the entrance nozzles. In passing through the wall shear layer and porous tube, the fluid will in general suffer a total pressure loss and a stagnation temperature increase, the latter because it contains fissionable material. Thus, the recirculation system must increase the total pressure of the fluid, and decrease its stagnation temperature.

The two devices which are to be proposed for this purpose are essentially heat engines, their energy source being in both cases the heat picked up by the bled fluid during its residence within the vortex tube, and their net work supplying the desired total pressure rise. Any heat engine must reject a considerable fraction of its input energy, as heat, at some temperature below that of its heat source. It will be assumed, for the present rocket application, that no external heat sink is available, so that all of

this heat must be rejected to the propellant. Since the propellant can only be raised to some temperature below that of the fluid entering the vortex tubes, its heat capacity is limited, and the total pressure rise which can be obtained is therefore also limited.

Gas turbine cycle:

The first device which will be considered is a rather conventional gas turbine cycle, shown schematically in Fig. 6. The fluid bled from the vortex tube expands through a turbine, which drives a compressor and a pump, then passes through a heat exchanger, where it rejects heat to the propellant. It is then compressed and re-enters the vortex tube. The propellant is raised from tank pressure to vortex entrance pressure by the pump, picks up heat from both the recirculated fluid and any solid parts of the reactor which must be cooled, then enters the vortex tube. The net flow into the system, which is handled by the pump, is equal to the net radial inflow through the vortex.

The following notation will be used:

T_t \equiv turbine inlet temperature

τ \equiv total temperature ratio

π \equiv total pressure ratio

η \equiv efficiency or effectiveness

ΔH \equiv enthalpy rise of propellant, per unit mass

$(1 + w_b)w_b / (1 + w_c)w_c$ \equiv ratio of recirculated to through mass flows

c_p \equiv specific heat at constant pressure of recirculating fluid

γ \equiv ratio of specific heats of recirculating fluid.

The values of τ , π , η , and ΔH for the various components of the cycle will be distinguished by subscripts as follows:

- t , turbine
- c , compressor
- v , vortex tube
- s , reactor solids
- h , heat exchanger .

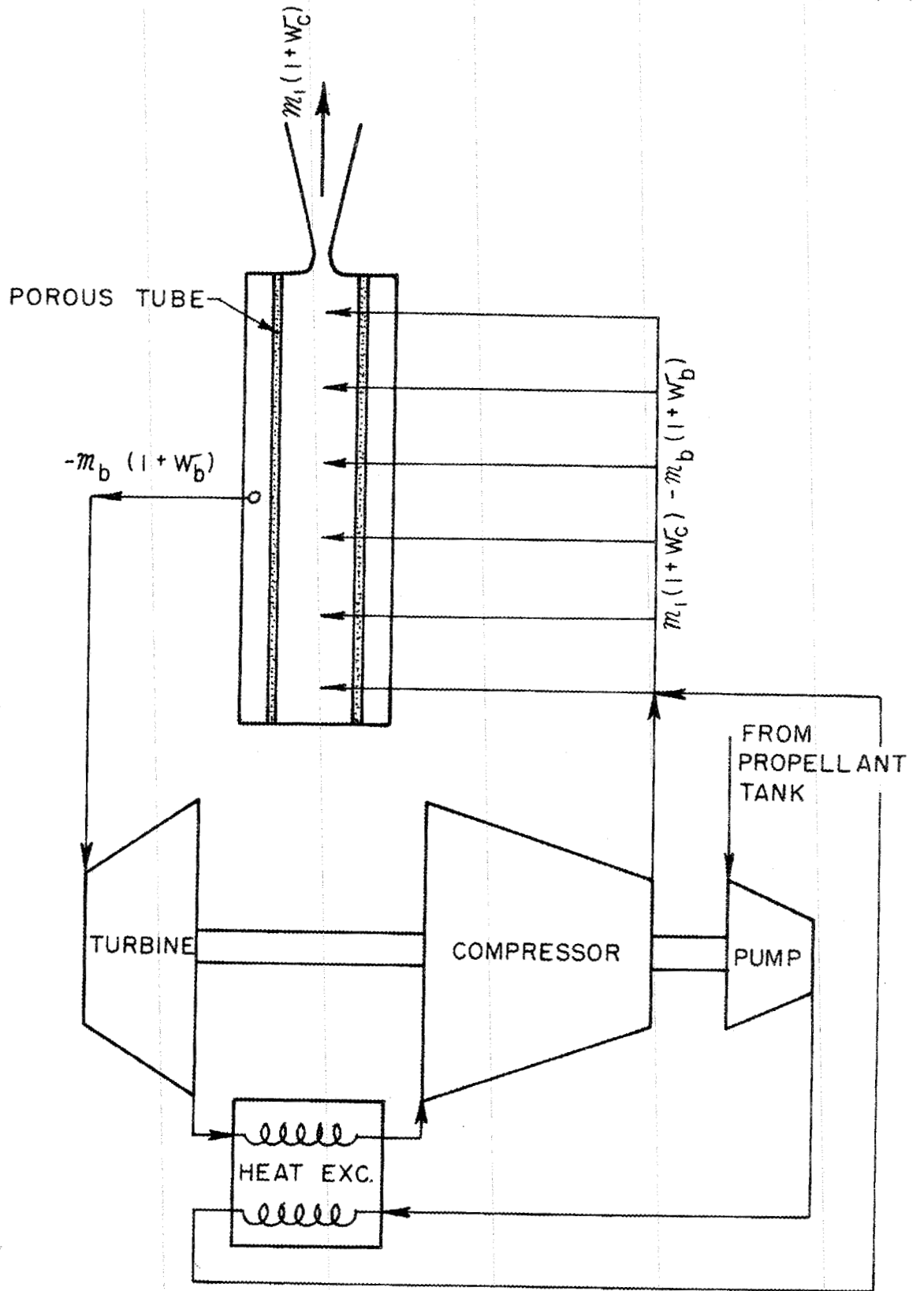


Fig. 6. Schematic of Gas-Turbine Driven Recirculation System.

Since the fluid recirculates, it is necessary that

$$\tau_c \tau_v \tau_t \tau_h = 1 \quad , \quad \text{I-(14)}$$

and

$$\pi_c \pi_v \pi_t \pi_h = 1 \quad . \quad \text{I-(15)}$$

A work balance for the turbine, compressor, and pump gives,

$$\tau_t = 1 - \tau_t \tau_h (\tau_c - 1) + \frac{(1 + w_c) \dot{m}_1}{(1 + w_b) \dot{m}_b} \left(\frac{\Delta H_p}{c_p T_t} \right) \quad . \quad \text{I-(16)}$$

The energy balance for the heat exchanger gives,

$$\tau_h = 1 + \frac{(1 + w_c) \dot{m}_1}{(1 + w_b) \dot{m}_b} \frac{1}{\tau_t} \left(\frac{\Delta H_h}{c_p T_t} \right) \quad . \quad \text{I-(17)}$$

According to the usual definitions of the efficiencies of the turbine and compressor, we have finally,

$$\tau_c = 1 + \frac{1}{\eta_c} \left(\pi_c \frac{\gamma - 1}{\gamma} - 1 \right) \quad \text{I-(18)}$$

and

$$\tau_t = 1 - \eta_t \left(1 - \pi_t \frac{\gamma - 1}{\gamma} \right) \quad . \quad \text{I-(19)}$$

Straightforward manipulation of these equations yields the following expression for the mass flow ratio:

$$\frac{(1 + w_c)}{(1 + w_b)} \left(\frac{\dot{m}_1}{\dot{m}_b} \right) \left(\frac{\Delta H_h}{c_p T_t \tau_t} \right) = \frac{\left(1 + \frac{\pi_c \frac{\gamma - 1}{\gamma} - 1}{\eta_c} \right) - \left\{ 1 + \eta_t \left[\left(\frac{1}{\pi_c \pi_v \pi_h} \right)^{\frac{\gamma - 1}{\gamma}} - 1 \right] \right\}^{-1}}{\frac{\pi_c \frac{\gamma - 1}{\gamma} - 1}{\eta_c} - \frac{\Delta H_p}{\Delta H_h}} \quad . \quad \text{I-(20)}$$

The factor $\Delta H_n / c_p T_t \zeta_t$ shows the limitation imposed on the mass flow ratio by the heat capacity of the propellant. If the enthalpy rise of the propellant in the heat exchanger can be increased, the mass flow ratio can be increased, since a smaller amount of propellant can provide the required heat capacity. The right side of Eq. (20) is plotted in Fig. 7, for $\Delta H_p = 0$, as a function of $\pi_v \pi_h$ and π_c .

It seems likely that $\pi_v \pi_h$ will be less than 0.5, this being the value which corresponds to the ratio of static to total pressures at a Mach number of unity. Thus, the lowest obtainable value of the quantity plotted in Fig. 7 is about 0.65.

The largest possible value of $\Delta H_n / c_p T_t \zeta_t$ is obtained when ΔH_n is the enthalpy rise of the propellant from tank conditions to the temperature $T_t \zeta_t$. This value can be attained only if ΔH_p is negligible and the effectiveness of the heat exchanger is unity; however, it serves to establish an upper limit to the mass flow ratio. These maximum possible values of $\Delta H_n / c_p T_t \zeta_t$ are shown in Fig. 8 for hydrogen. The initial state has been taken as the liquid at its normal boiling point. Since the values of $\Delta H_n / c_p T_t \zeta_t$ are very close to unity, a reasonable lower limit for $(1 + w_c) \mathcal{M}_1 / (1 + w_b) \mathcal{M}_b$ is 0.65 or 0.70, and the greatest obtainable mass flow ratio is 1.4 to 1.5. The gas turbine system is therefore at best marginal, according to the criteria established by the diffusion and boundary layer stabilization processes, which require mass flow ratios of two and unity, respectively.

In order that the cycle operate at a point on Fig. 7, a certain amount of heat must be supplied to it. This heat input may be expressed in terms of the temperature ratio across the vortex tube, ζ_v . From Eqs. (14) to (19),

$$\zeta_v = \frac{1}{1 + \left(\frac{1 + w_c}{1 + w_b} \right) \left(\frac{\mathcal{M}_1}{\mathcal{M}_b} \right) \frac{\Delta H_n}{c_p T_t \zeta_t} \left\{ 1 + \eta_t \left[\left(\frac{1}{\pi_c \pi_v \pi_h} \right)^{\frac{\gamma - 1}{\gamma}} - 1 \right] \right\} \left(1 + \frac{\Delta H_p}{\Delta H_n} \right)} \quad \text{I-(21)}$$

UNCLASSIFIED
ORNL-LR-DWG 30568

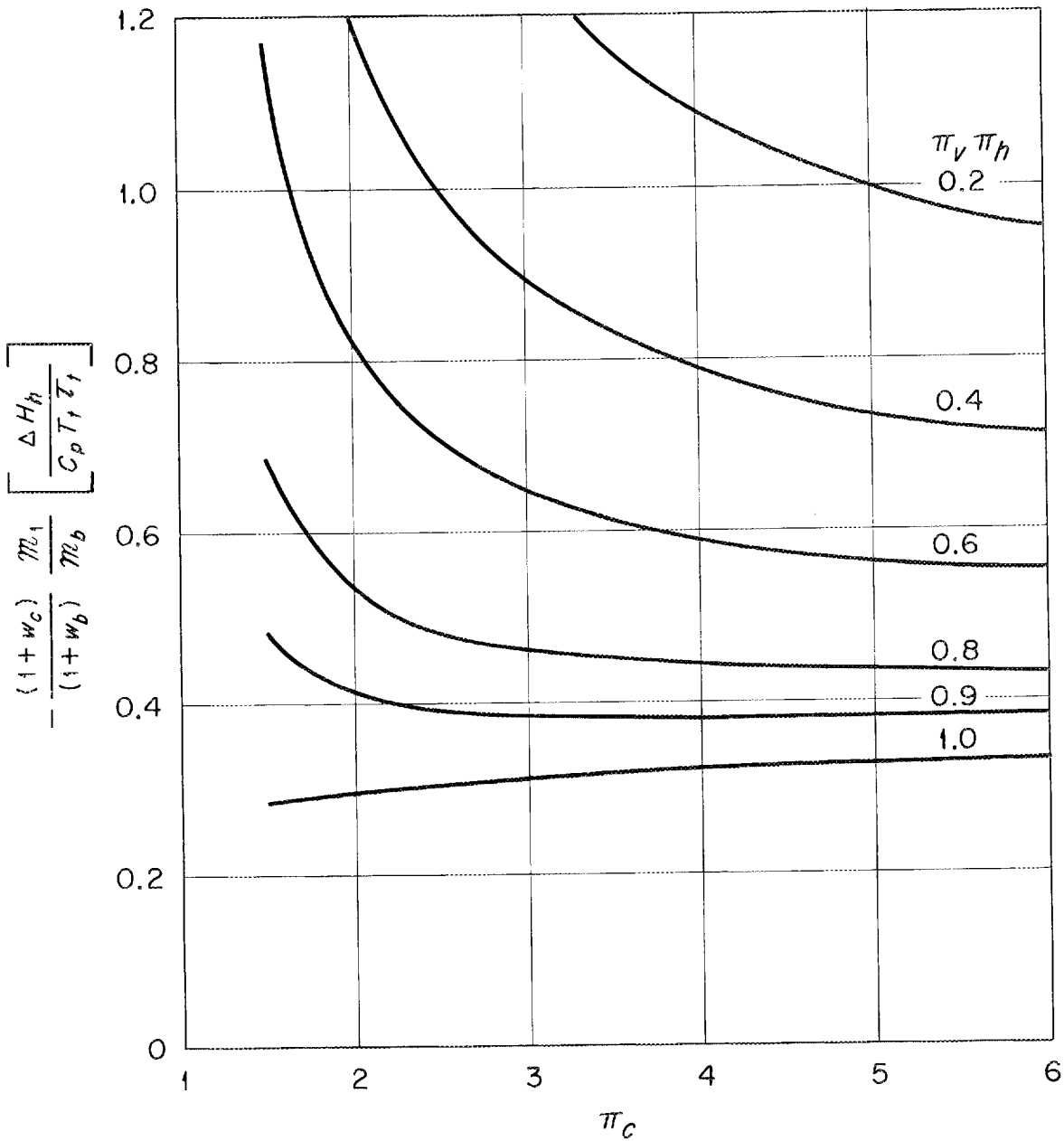


Fig. 7. Permissible Mass Flow Ratios for Gas-Turbine Recirculation System, as Function of Compressor Pressure Ratio and Total Pressure Loss Ratio.

UNCLASSIFIED
ORNL-LR-DWG 30569

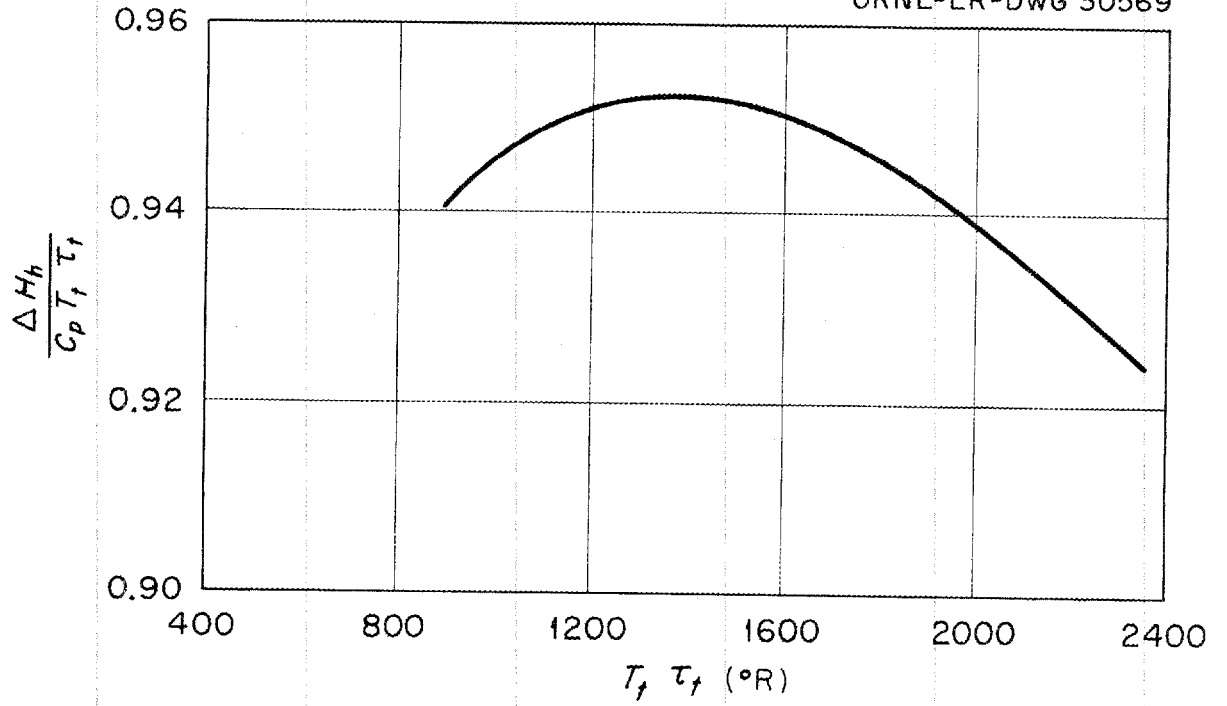


Fig. 8. Variation of Maximum Dimensionless Heat Exchanger Enthalpy Rise with Turbine Outlet Temperature, for Hydrogen.

As is shown in Fig. 9, the temperature ratio required for the mass flow ratios from 1.4 to 1.5 is about 2.0. This figure does not impose an important limitation on the system unless it is so low that it becomes impossible to circulate the mixture of propellant and fissionable material through the vortex tube without its temperature ratio exceeding the indicated value.

Propellant turbine cycle:

The second cycle which will be considered is one in which only the through flow of propellant passes through the turbine. Such a scheme is shown in Fig. 10. The propellant is pressurized by a pump, picks up heat from the circulating fluid, then expands through the turbine and passes into the vortex tubes. The recirculating fluid passes through the heat exchanger and compressor only.

Using the same notation as for the gas turbine cycle, we must have,

$$\tau_c \tau_v \tau_h = 1 \quad \text{I-(22)}$$

$$\eta_c \eta_v \eta_h = 1 \quad \text{I-(23)}$$

The energy balance for the pump, turbine, and compressor is

$$-\frac{\dot{m}_1(1+w_c)}{\dot{m}_b(1+w_b)} (\Delta H_t - \Delta H_p) = c_p T_h \tau_h (\tau_c - 1), \quad \text{I-(24)}$$

where T_h is the temperature of the circulating fluid entering the heat exchanger. The energy balance for the heat exchanger gives,

$$-\frac{\dot{m}_1(1+w_c)}{\dot{m}_b(1+w_b)} \Delta H_h = c_p T_h (1 - \tau_h) \quad \text{I-(25)}$$

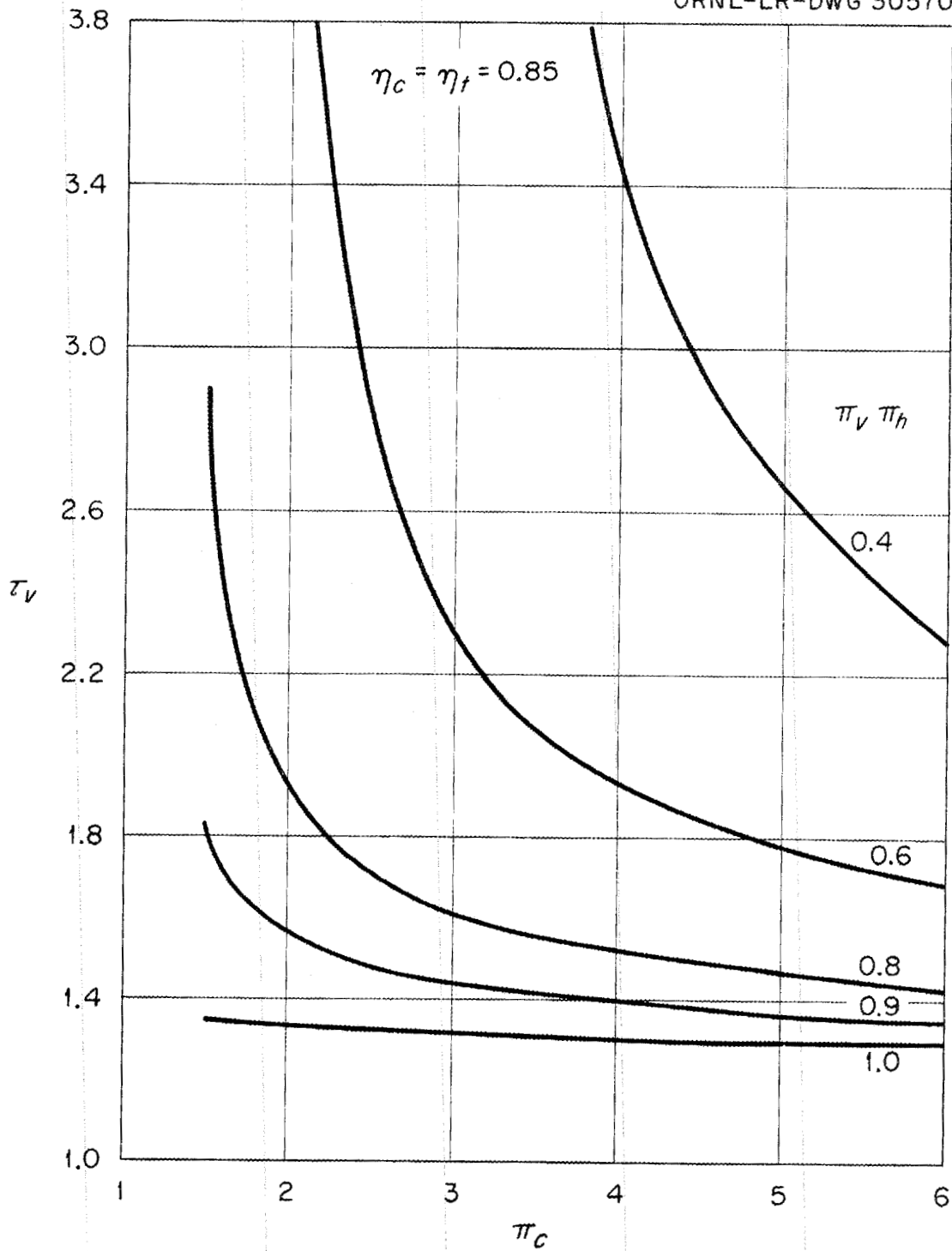


Fig.9. Vortex Tube Temperature Ratios Required by Gas-Turbine Recirculation Systems.

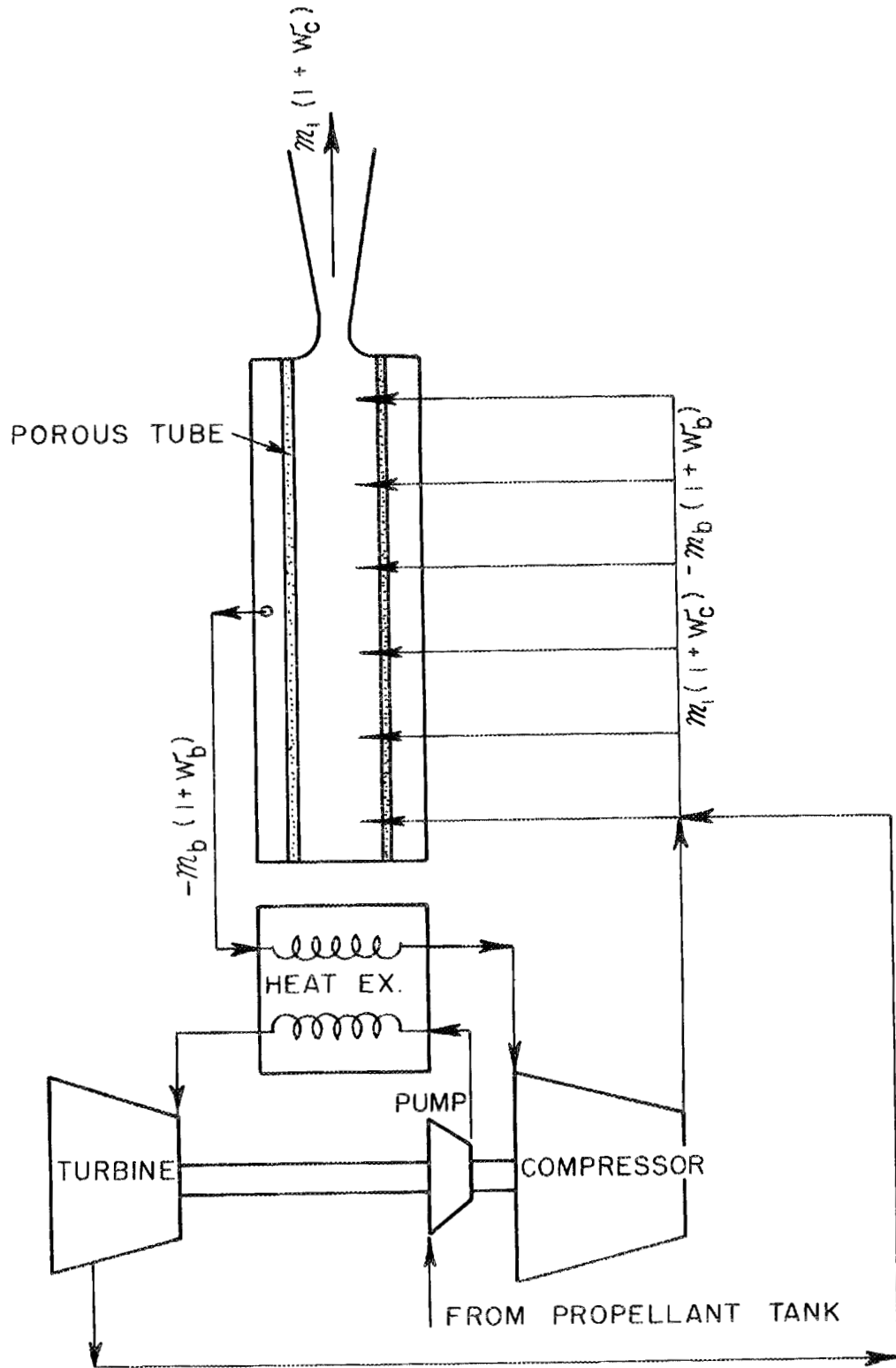


Fig. 10. Schematic of Propellant-Turbine Driven Recirculation System.

From these equations, it is readily shown that,

$$\frac{\mathcal{M}_1(1+w_c)}{\mathcal{M}_b(1+w_b)} \left(\frac{\Delta H_h}{c_p T_h} \right) = \frac{\left(\frac{1}{\pi_v \pi_h} \right)^{\frac{\gamma-1}{\gamma}} - 1}{\eta_c \left(\frac{\Delta H_t}{\Delta H_h} - \frac{\Delta H_p}{\Delta H_h} \right) + \left[\frac{1}{\pi_v \pi_h} \right]^{\frac{\gamma-1}{\gamma}} - 1} \quad I-(26)$$

It is clear that $\Delta H_h/c_p T_h$ plays the same role for this cycle that $\Delta H_h c_p T_t \tau_t$ does for the gas turbine cycle, i.e., it shows the limitation of the mass flow ratio by the propellant heat capacity.

The right side of Eq. (26) is shown in Fig. 11 as a function of $\Delta H_t/\Delta H_h$ and $\pi_v \pi_h$. Rather large mass flow ratios are obtainable for $\Delta H_t/\Delta H_h$ equal to 0.5 or more. However, such large values of $\Delta H_t/\Delta H_h$ imply small values of π_t , since

$$\pi_t = \left[1 - \left(\frac{\Delta H_t}{\Delta H_h} \right) \left(\frac{\Delta H_h}{c'_p T_h} \right) \left(\frac{T_h}{T_t} \right) \right]^{\frac{\gamma'}{\gamma' - 1}}, \quad I-(27)$$

where c'_p and γ' are values for the pure propellant. If, for example, $\Delta H_h/c'_p T_h$ and T_h/T_t are both unity, and $\Delta H_t/\Delta H_h$ is 0.5, π_t is about 0.09. Such low values of π_t cannot be tolerated, since the vortex feed pressure is already very high(1).

For $\pi_v \pi_h = 0.5$, and the minimum satisfactory value of $\mathcal{M}_b(1+w_b)/\mathcal{M}_1(1+w_c)$, i.e., 2.0, we find $\Delta H_t/\Delta H_h = 0.25$ and $\pi_t = 0.37$. Thus, even to obtain a mass flow ratio of 2.0, the pumping pressure must be increased by a factor of about 2.7.

The temperature ratio required for operation under the conditions implied by Fig. 11 is given by,

$$\tau_v = \frac{1}{\left\{ 1 + \frac{1}{\eta_c} \left[\left(\frac{1}{\pi_v \pi_h} \right)^{\frac{\gamma-1}{\gamma}} - 1 \right] \right\} \left\{ 1 + \frac{\mathcal{M}_1(1+w_c)}{\mathcal{M}_b(1+w_b)} \frac{\Delta H_h}{c_p T_h} \right\}}, \quad I-(28)$$

UNCLASSIFIED
ORNL-LR-DWG 30571

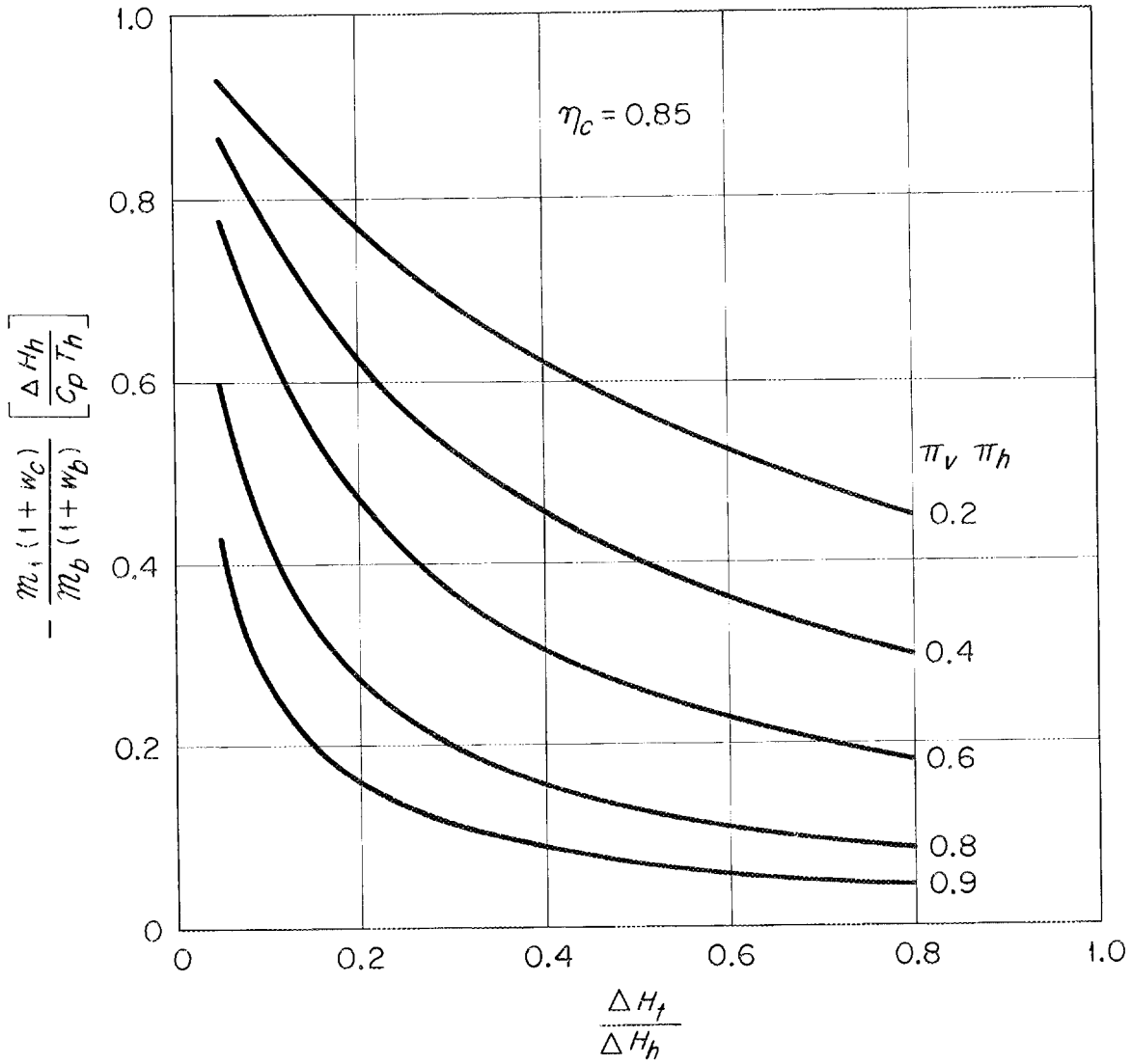


Fig. II. Permissible Mass Flow Ratios for Propellant-Turbine Recirculation System, as Function of Ratio of Turbine and Heat Exchanger Enthalpy Changes and Total Pressure Loss Ratio.

and is shown in Fig. 12. As for the gas turbine cycle, the value of τ_v does not constitute a limitation on the cycle unless it is so small that the fluid cannot be circulated through the vortex tubes without its temperature ratio exceeding τ_v .

Conclusions:

On the basis of the preceding analyses, the following conclusions seem warranted.

1. Laminar vortices having tangential velocities greater than one-half the inviscid value can be generated by providing uniform wall suction, with ratios of bled mass flow to radial mass flow of unity or higher.

2. The tendency of the radial outflow through the tube wall to sweep the heavy gas from the vortex is reduced as the above mentioned mass flow rate increases. For a mass flow ratio of 2, the heavy to light gas density ratio at the tube wall is less than twice that at the vortex periphery.

3. A gas turbine cycle operating with the recirculating fluid as a working medium is capable of recirculating the fluid at mass flow ratios up to 1.5 if the total pressure ratio across the vortex tube is 0.5.

4. A propellant turbine cycle is capable of producing a mass flow ratio of 2.0 at the total pressure ratio of 0.5, if the pumping pressure can be increased to 2.7 times the vortex feed pressure.

5. From the above four conclusions, it is probable that a recirculation system can be devised, which will enable laminar vortices, of sufficient strength for separation, to be produced.

UNCLASSIFIED
ORNL-LR-DWG 30572

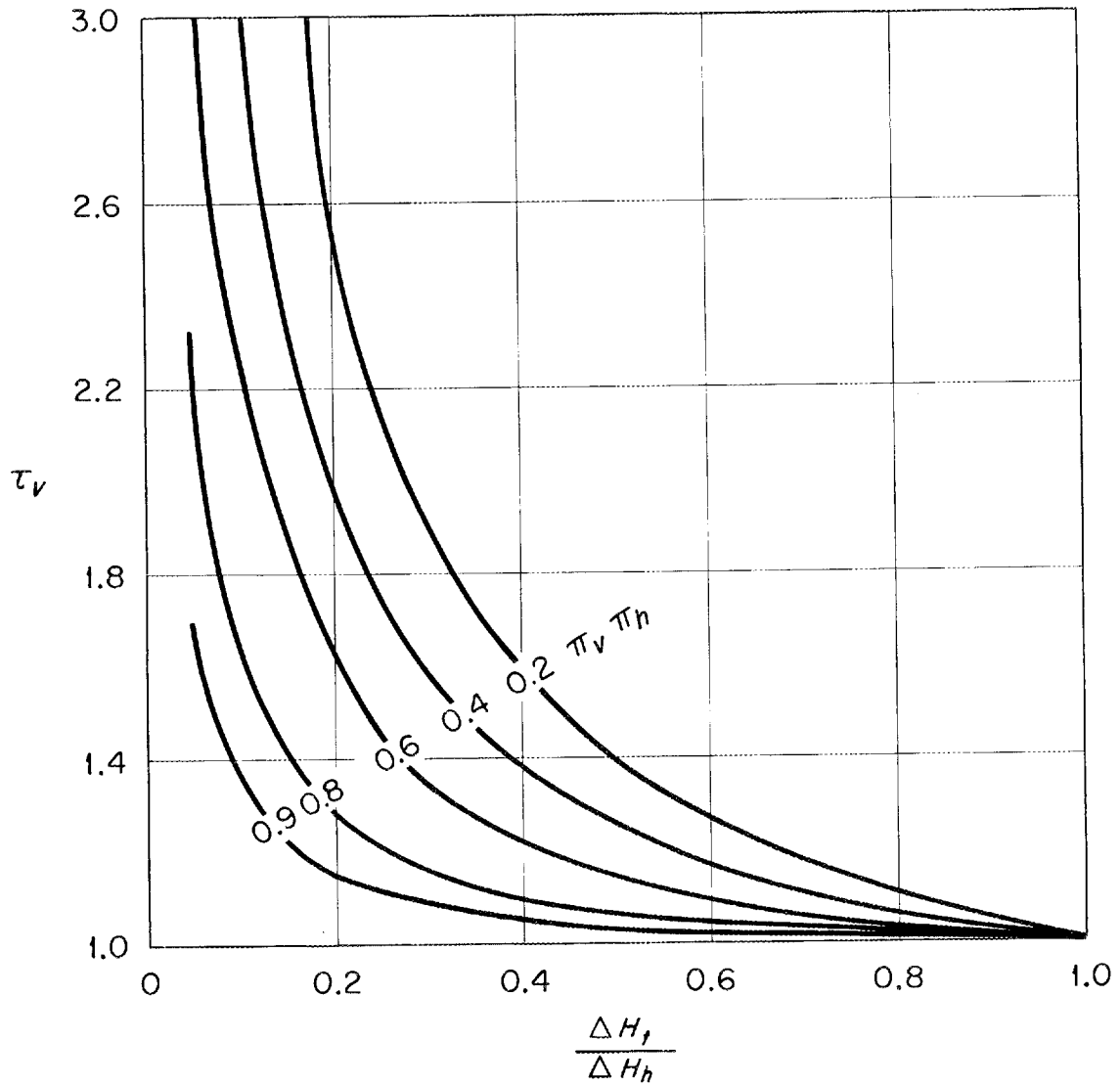


Fig.12. Vortex Tube Temperature Ratios Required by Propellant-Turbine Recirculation System.

SECTION II

Criticality

Introduction:

The criticality problem for vortex reactors is unusual in that the reactor weight is of extreme importance. In addition to its influence on the performance of a rocket vehicle through the thrust to weight ratio of the rocket reactor, the criticality requirement in a sense determines the size of vehicle to which a given rocket reactor is applicable. Thus, vortex reactors are not scaleable in the usual sense. A characteristic length has been introduced by the neutron transport processes.

Because of the rather low fissionable material concentrations allowed by the vortex-separation process, the sizes and weights of vortex reactors tend to be large, in the sense that the vortex reactor is suitable for very large rocket vehicles. The fuel concentration can be increased, and the reactor weight reduced, by increasing the pressure in the vortex tubes, but the containment problem is then aggravated. It appears that, for a given vortex tube design, it will generally be desirable to select the reactor configuration so as to minimize the reactor weight. Thus, the approach taken in the present calculations is to minimize the reactor weight, by varying the reactor configuration, for fixed vortex tube designs. The vortex tube designs which have been selected as examples are those given in Table I, p. 61, of Ref. 1.

Since the calculations are exploratory, hence parametric in nature, a simple two-group, two-region nuclear model is used. The reactor core is assumed to be a cylindrical matrix of vortex tubes in pure moderator, of diameter equal to the length of the tubes. A beryllium reflector of uniform thickness surrounds the core on all sides. Thus, for a given vortex tube design, the characteristics of the reactor are determined by the reflector thickness and the ratio of tube volume to total core volume, which will be called the moderator void fraction.

Derivation of Nuclear Constants from Separation Calculation:

Representative nuclear constants for the two-group, two-region criticality calculations were derived from the examples of Ref. 1, Table I, as follows.

Thermal average fission and absorption cross sections were computed for reactor cores consisting of either graphite, hydrogen, and plutonium or beryllium, hydrogen, and plutonium. The concentrations of hydrogen and plutonium in the vortex tubes were determined for each vortex tube design, from the data given in Ref. 1, Table I. Then for an assumed moderator void fraction, the cross sections were computed for a homogenized, uniform core. It was assumed, in computing the thermal average cross sections, that the thermal neutrons were distributed in energy according to a Maxwell-Boltzmann distribution at the temperature of the moderator, which in turn was taken as the vortex tube entrance temperature.

Examples were given in Ref. 1 of vortex configurations capable of producing two different temperature ratios. The first three examples were for vortex entrance and exit temperatures of 4500 and 7020°R, while the last three were for entrance and exit temperatures of 2420 and 10,000°R. The three cases for each temperature ratio were for values of w_m equal to 0.5, 1.0 and 4.0, where w_m is the maximum value of the ratio of fissionable gas density to hydrogen density occurring in the tube.

It was found that for all these cases, the macroscopic fission cross section of the homogenized reactor core depended on the product of w_m and the vortex exit pressure, p_{oc} , in the simple way shown in Fig. 13. For a given moderator void fraction the dependence of Σ_f on w_m is small for w_m between zero and unity, but becomes appreciable for w_m equal to four. The variation of the infinite medium multiplication constant, k_{∞} , with Σ_f is shown in Fig. 14 for the same cases. By combining Figs. 13 and 14, k_{∞} could be given as a function of $p_{oc} w_m$ also.

For the two group - two region calculations, representative cases were selected for the two moderators as indicated by the points in Fig. 14.

A moderator void fraction of 0.6 was assumed in Figs. 13 and 14. To determine the influence of the void fraction, reactors with a fixed vortex design, (case 5 of Ref. 1, Table I, with $p_{oc} = 200$ atm) and various void fractions, were also computed.

The neutron diffusion coefficient for the thermal group was taken as the moderator diffusion coefficient, corrected for the moderator void fraction.

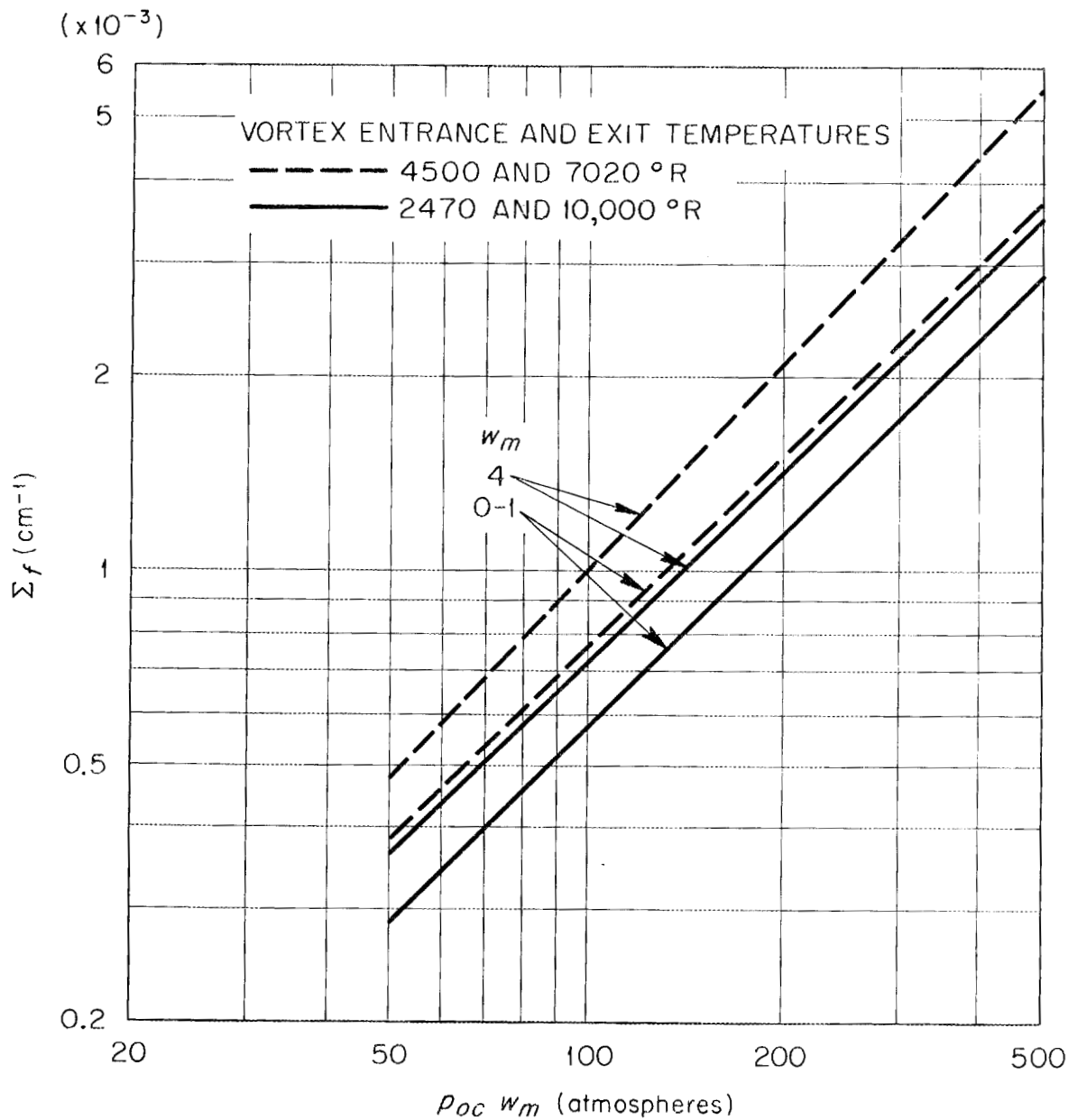


Fig.13. Variation of Macroscopic Fission Cross-Section with Product of Vortex Outlet Pressure and Maximum Value of Ratio of Fuel Density to Propellant Density, for Typical Vortex Reactors.

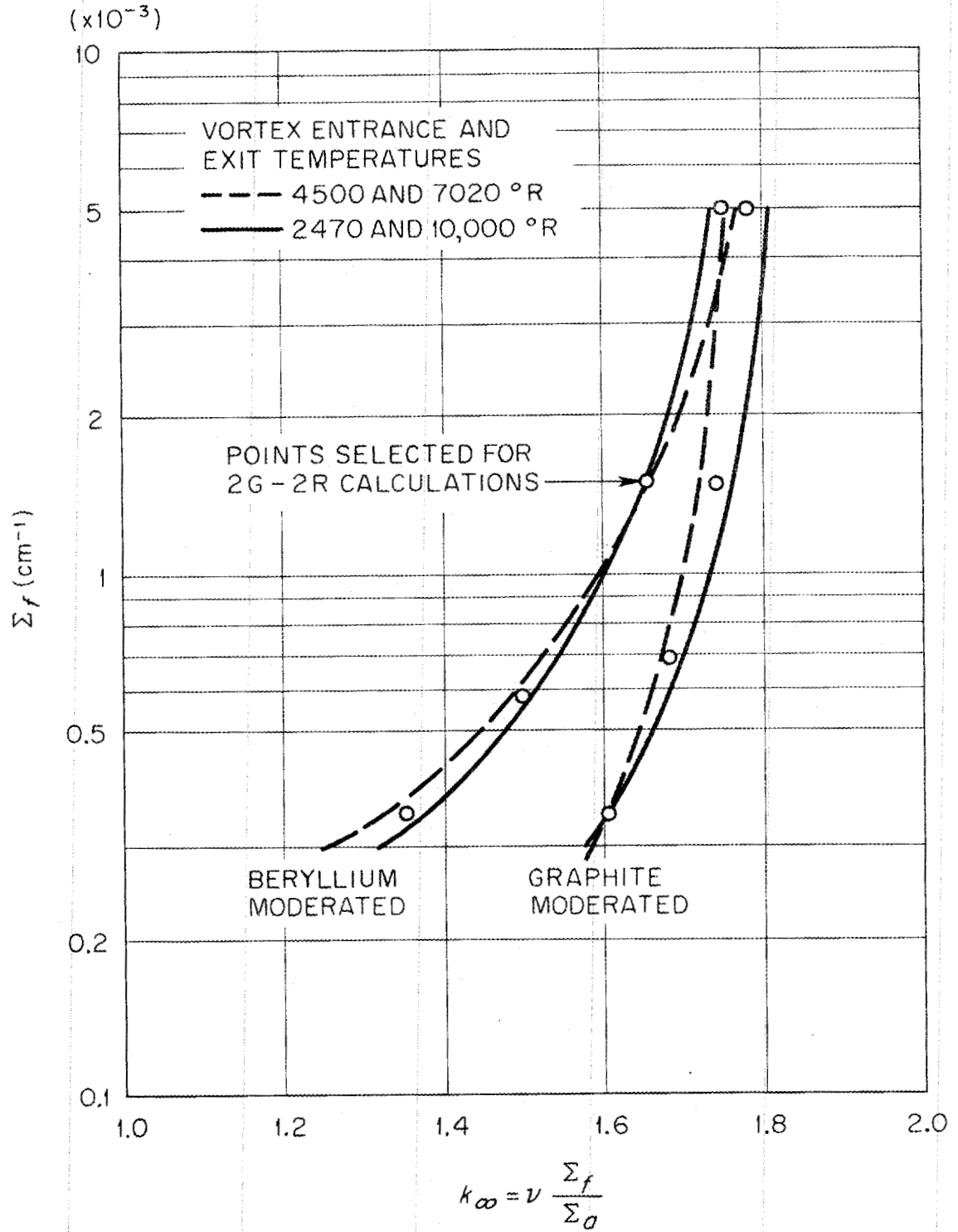


Fig. 14. Variation of Infinite Medium Multipli-
cation Constant with Macroscopic Fission Cross-Section
for Typical Vortex Reactors.

In choosing the nuclear constants for the fast neutron group, several simplifying assumptions were made. The resonance escape probability was taken as unity, and fast fission was neglected. The cross section for removal of neutrons from the fast group to the thermal group was taken as the diffusion coefficient divided by the Fermi age to Indium resonance. The age to Indium resonance was selected because of the high thermal neutron temperatures envisioned. The fast diffusion coefficient and the age were assumed to be those for pure moderator, corrected for the void fraction.

Reactor code:

The code used for computing the fully reflected, cylindrical reactors, consists of a three group, three region, one dimensional code, modified to two-groups and two-regions for this case, and a three-dimensional reflector savings program. The three-group, three region code has been described in Ref. 3. Since a description of the reflector savings program is not available in the literature, it will be briefly described here.

Multiplication constants are computed for two series of reactors, one series consisting of side reflected cylinders with bare ends, the other of end reflected cylinders with bare sides. In each case the cross section in the reflected dimension is the same as that of the fully reflected reactor for which the multiplication is to be found. By an iterative procedure, the code determines the height and diameter, respectively, of the side and end reflected cylinders of the two series which have the same multiplication constant as a bare reactor with this same height and diameter. The multiplication constant which is common to the bare cylinder, end reflected cylinder and side reflected cylinder is then taken as the multiplication constant for the fully reflected cylinder.

The iterative procedure is as follows. A height is assumed for the side reflected cylinder, and its multiplication constant computed. The diameter of a bare reactor with the same height and multiplication is then found. The multiplication is then computed for an end reflected reactor with this diameter. Finally, the height of a bare reactor with the same diameter and multiplication

is found. This height is then taken as an improved estimate for the height of the side reflected cylinder, and the procedure is repeated until the multiplication constants for the end and side reflected reactors agree.

Results:

The variation of reactor core plus reflector weight with reflector thickness is shown in Fig. 15 for each of the core compositions indicated by points on Fig. 14, and for a moderator void fraction of 0.6. For given core composition, the minimum weight occurs for reflector thicknesses of about 20 cm for the graphite cores and about 10 cm for the beryllium cores. For each value of Σ_f , the minimum weight beryllium core reactor is considerably lighter than the minimum weight graphite reactor. This difference is due to the better neutron moderating properties of beryllium as compared to graphite.

Critical core radii are shown in Fig. 16 for the same cases shown in Fig. 15. From a comparison of the two figures it is clear that the minimum reactor weight is attained for a reflector thickness considerably below the value which is effectively infinite. This is due in part to the fact that the core density is only about 0.4 of the reflector density for the beryllium cores, and even less for the graphite cores.

That the higher values of Σ_f , and the lower reactor weights, shown in Fig. 15, correspond to very high vortex-tube pressures can be seen from Fig. 13. The lowest reactor weight shown, 4800 lbs, requires that $p_{oc} w_m$ be equal to about 500 atm. It was pointed out in Ref. 1 that, for $w_m = 4$, this pressure level in the tubes would require a pumping pressure of about 1000 atm.

Critical masses are given in Fig. 17 for the minimum weight reactors from Fig. 15. The masses are quite low, as a result of two effects. First, the reactor core has been assumed to be free of structural poisons. Second, the fission cross section of plutonium actually increases with neutron temperature, up to about 1600°K, while the absorption cross sections of graphite, beryllium, and hydrogen decrease.

The effects of void fraction on reactor core plus reflector weight and core radius are shown in Figs. 18 and 19, for a core composition which gives $\Sigma_f = 1.15 \times 10^{-3}$ and $k_{\infty} = 1.74$ and 1.62 respectively for graphite and beryllium

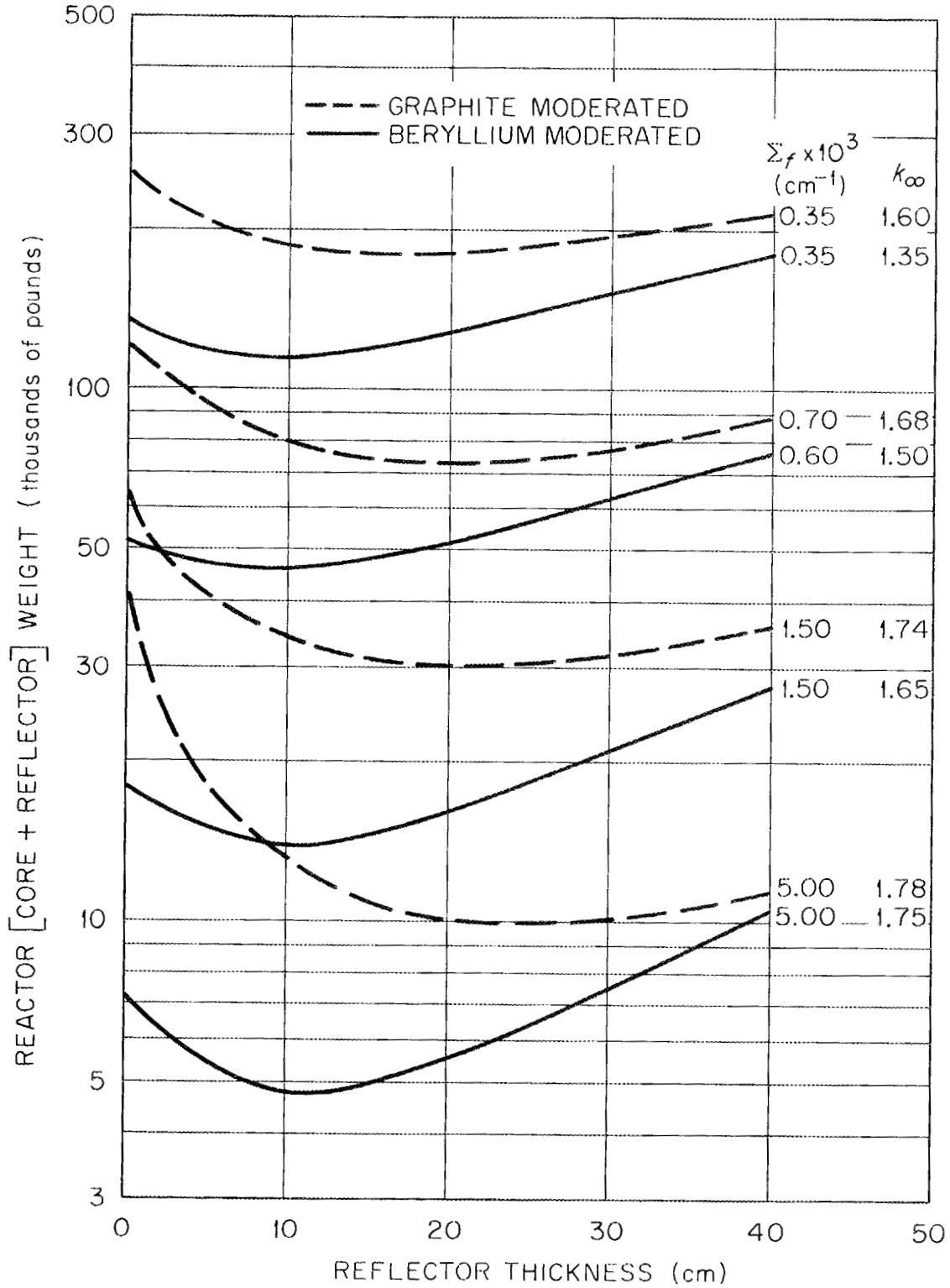


Fig.15. Variation of Reactor (Core plus Reflector) Weight with Reflector Thickness for Typical Graphite and Beryllium Moderated Reactors.

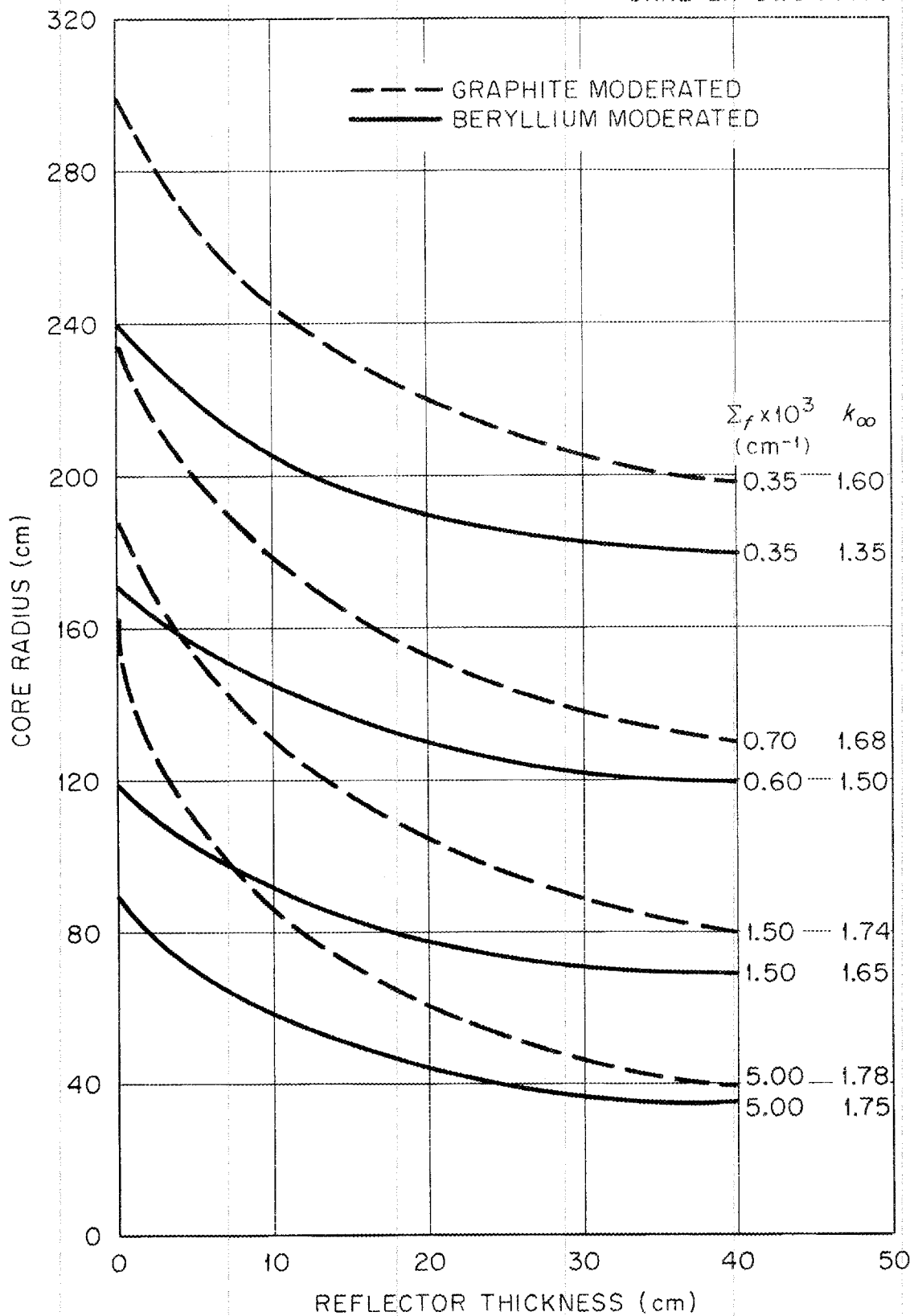


Fig. 16. Variation of Core Radius with Reflector Thickness for Typical Reactors.

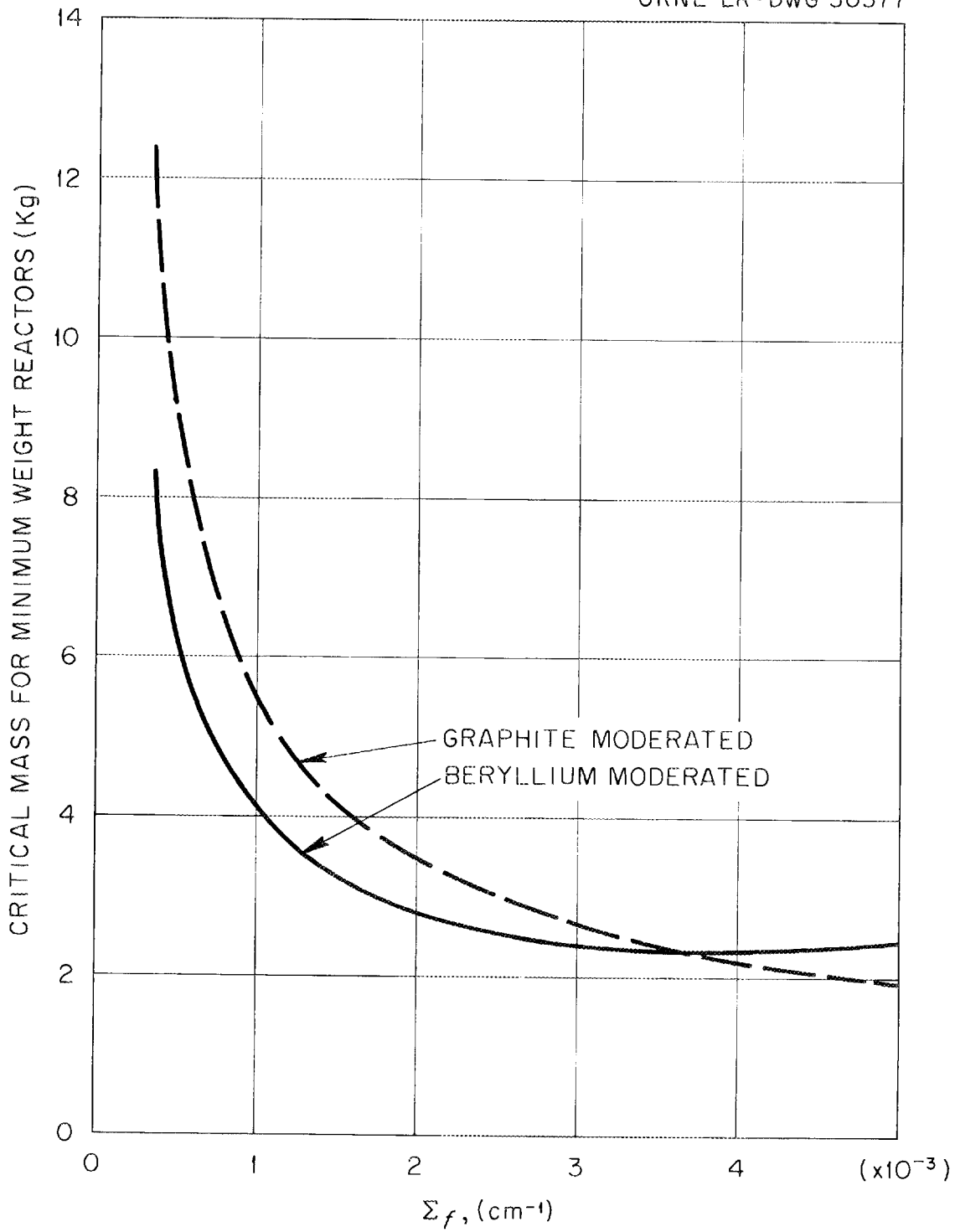


Fig.17. Variation of Critical Mass with Macroscopic Fission Cross Section for Minimum Weight Reactors.

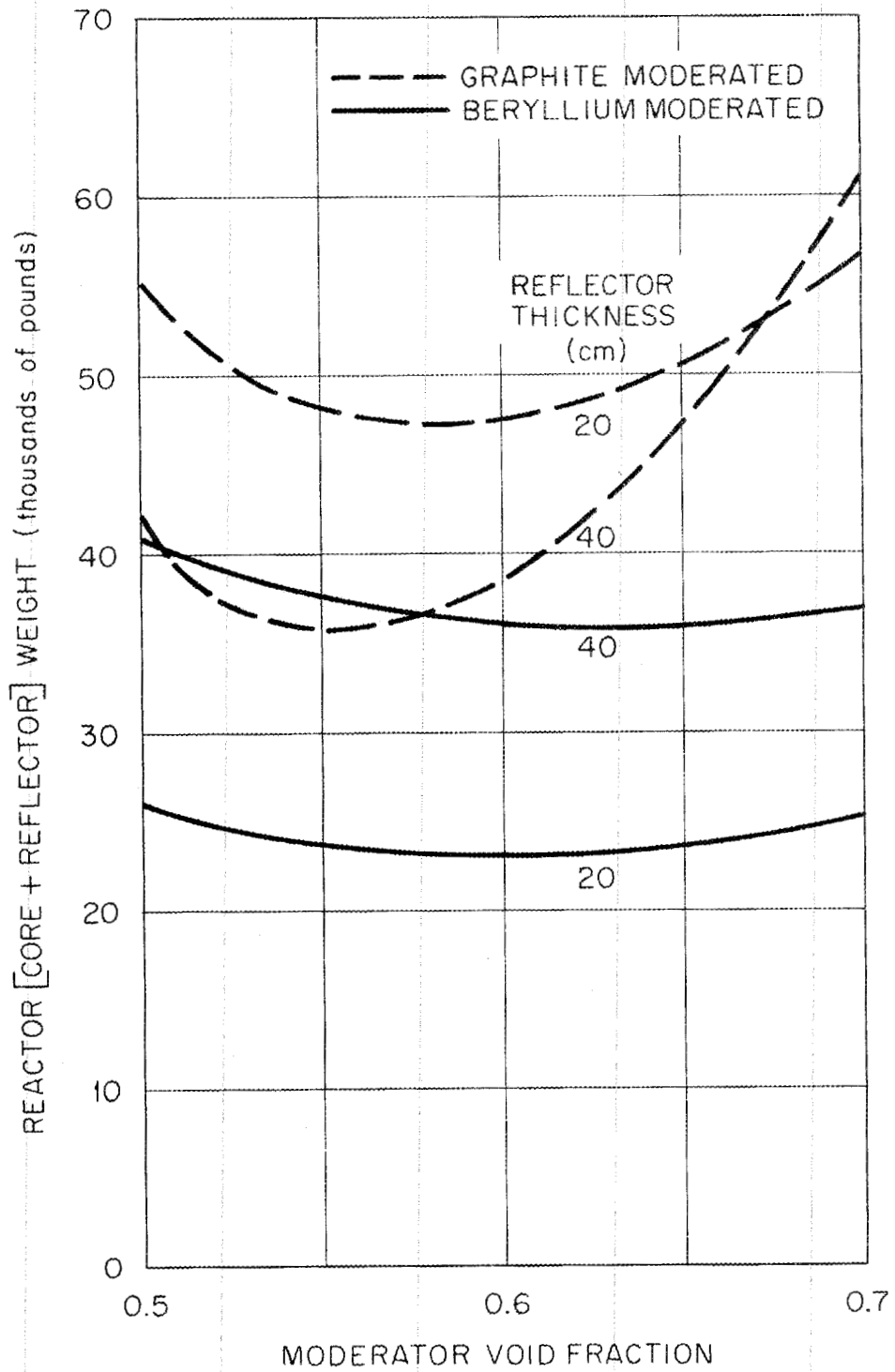


Fig.18. Variation of Reactor (Core plus Reflector) Weight with Moderator Void Fraction for Typical Reactors.

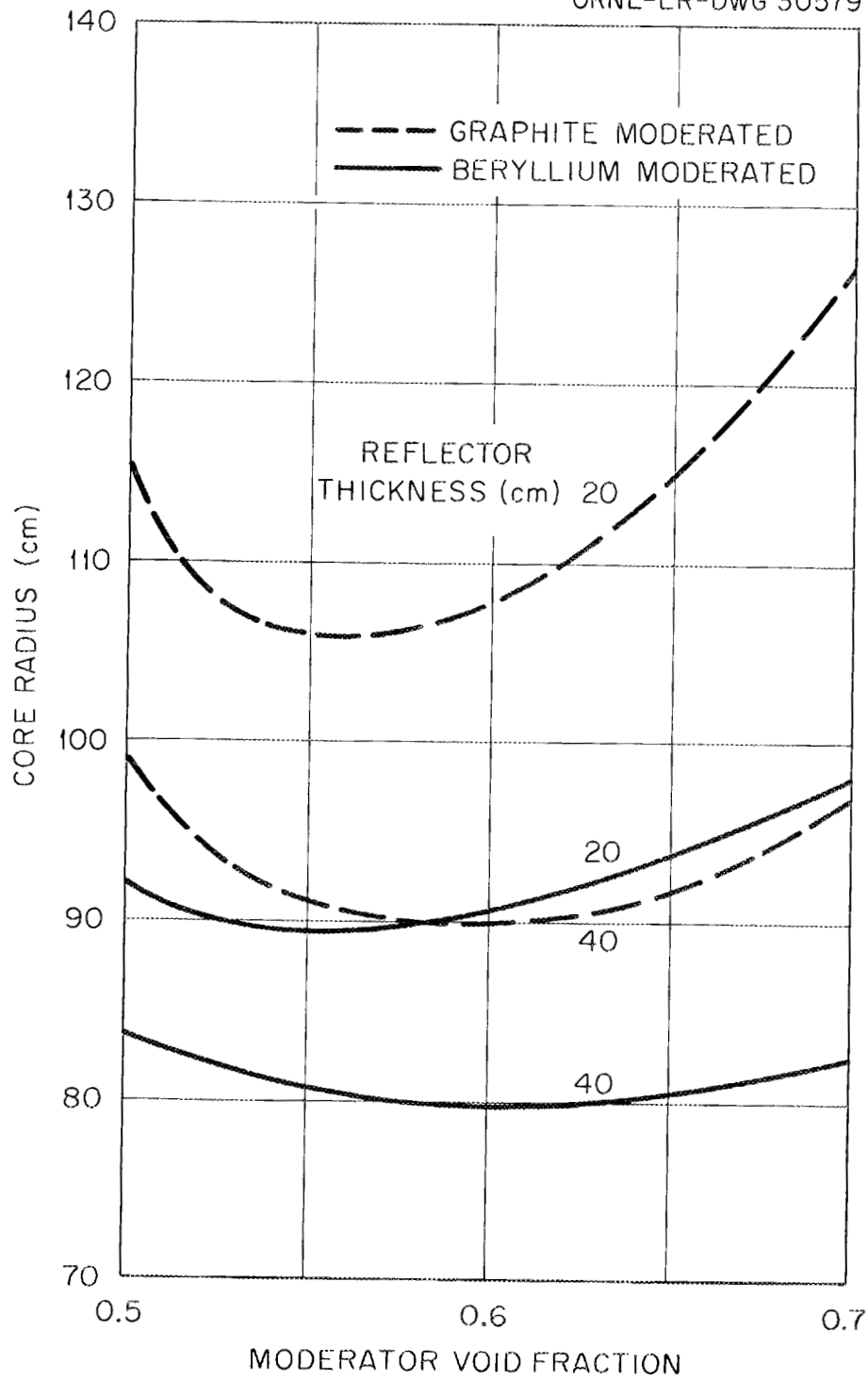


Fig.19. Variation of Core Radius With Moderator Void Fraction for Typical Reactors.

moderators and a void fraction of 0.6. Neither the weight nor the core radius are very sensitive to the void fraction for the cases shown. They would be somewhat more sensitive for thinner reflectors, however.

Conclusions:

The principal conclusion to be drawn from these simplified criticality calculations is that vortex reactors of reasonable size and weight can be obtained if the pressure and maximum fuel to hydrogen density ratio in the tubes are such that $p_{oc} w_m$ is greater than about 100, and if the core is free of structural poisons. Under these conditions, reflector thicknesses of about 20 and 10 cm give the lowest reactor weights for graphite and beryllium cores. The optimum moderator void fraction is between 0.5 and 0.6 for both moderators.

SECTION III

Gaseous Fissionable Compounds
for Vortex Reactors

Introduction:

It was implicitly assumed in Ref. 1 that some compound of plutonium, or uranium, could be found, which it would be possible to hold in gaseous form under the desired conditions. Rather high concentrations of fissionable material must be held at very high temperatures and under reducing conditions, if hydrogen is to be used as propellant. There is some doubt as to whether any material can be found which will satisfy these requirements, since the compounds of uranium and plutonium which are stable at high temperatures are neither very volatile nor very resistant to reduction by hydrogen.

If there is any appreciable tendency toward reduction of the fissionable material by hydrogen, this tendency will be increased by the separative effect of the vortex field, which will tend to separate the products of the reduction from the reactants. A quantitative description of this effect involves a very complicated multi-component diffusion problem, with chemical reactions between the components, and will not be attempted at the present time. Rather, the requirement of chemical equilibrium will be indicated by giving the concentrations of reduction products which must be maintained, in order that the reduction be restricted to the desired extent.

Possible fuel carriers:

Of the many compounds of plutonium and uranium, only a few appear to be promising for the present application. These are the oxides, halides, the metals themselves, and possibly the hydrides. The hydrides are eliminated immediately on the basis of instability at high temperatures. The decomposition pressure of PuH_2 at $2000^{\circ}K$ is about $5000 \text{ atm}^{(4)}$. The halides and oxides of plutonium and uranium are quite similar in behavior, but plutonium has nuclear characteristics somewhat superior to those of uranium. Furthermore, the volatility of metallic plutonium is much higher than that of metallic uranium, so it seems sufficient to consider metallic plutonium, the plutonium halides, and plutonium oxides as the most promising fuel carriers. Since the higher halides are quite readily reduced to the tri-halides by hydrogen at only slightly elevated temperatures ($225-600^{\circ}C$ for PuF_3)⁽⁵⁾, only the tri-halides will be considered.

Volatility:

The concentrations at saturation are shown as functions of temperature in Fig. 20, for the interesting fuel carriers. The curve for Pu Cl₃ would lie between those for PuF₃ and PuBr₃, but has been omitted because of the high neutron absorption cross section of chlorine.

These curves have been computed from the Clausius-Clapeyron equation,

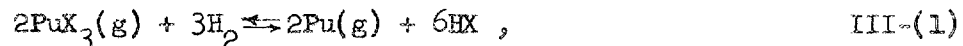
$$\log p = - \frac{L_0}{RT} + c ,$$

where L₀ is the latent heat of vaporization. The empirical values of L₀ and c for PuF₃ and PuBr₃ were obtained over temperature ranges of 1440 to 1770 and 929 to 1100 °K⁽⁶⁾, respectively, and have not been corrected for the temperature dependence of L₀. The data for PuO₂ are for the vapor in equilibrium with solid⁽⁷⁾, at temperatures up to 1800°C, hence, the vapor pressure at the higher temperatures is probably overestimated for PuO₂. The range of applicability of the data for Pu was not given in Ref. 8.

Criticality calculations⁽¹⁾ have indicated that fissionable material concentrations of at least 0.5x10¹⁸ cm⁻³ are necessary in the low temperature regions of the vortex tube. Thus, if a metallic tube structure is to be used, PuBr₃ is probably the only fuel carrier with sufficient volatility. If the lowest temperature in the tube is of the order of 2100°K or above, PuF₃ is sufficiently volatile; however, 3000°K is necessary to allow the desired concentration if metallic Pu is the fissionable gas.

Chemical equilibrium:

If the reaction of the fuel carrier with hydrogen,



proceeds so far toward the right that the concentration of Pu(g) exceeds that corresponding to the plutonium vapor pressure at the existing temperature, the plutonium will condense. Thus, an upper limit is placed on the permissible concentration of Pu by its vapor pressure. The permissible concentration of PuX₃ is related to the concentrations of Pu, HX, and H₂ by the equilibrium constant,

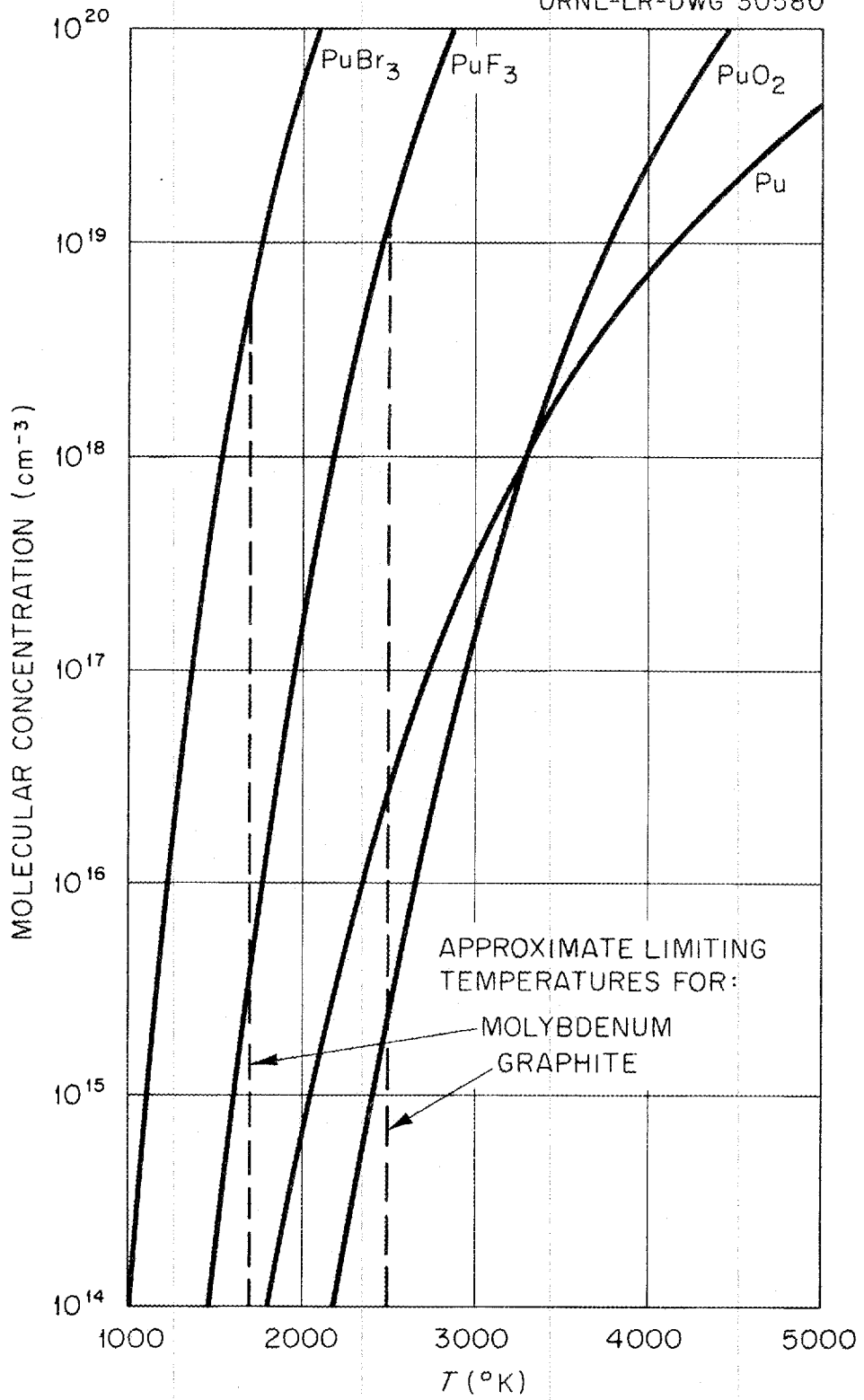


Fig. 20. Vapor Pressure Limited Concentrations for Possible Fuel Carriers.

$$K_p = \frac{(\text{Pu})^2(\text{HX})^6}{(\text{PuX}_3)^2(\text{H}_2)^3}, \quad \text{III-(2)}$$

where (X) is the partial pressure of X, in atmospheres. Equation (2) may be re-written as,

$$\frac{(\text{HX})^2}{(\text{H}_2)} = K_p^{1/3} \left(\frac{n_{\text{PuX}_3}}{n_{\text{Pu}}} \right)^{2/3}.$$

If n_2 is the total fissionable material concentration, and $n_{\text{Pu},v}$ is the concentration of plutonium at saturation, then we must have

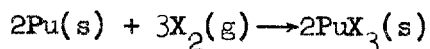
$$\frac{(\text{HX})^2}{(\text{H}_2)} \geq K_p^{1/3} \left(\frac{n_2}{n_{\text{Pu},v}} - 1 \right)^{2/3}, \quad \text{III-(3)}$$

in order that the plutonium shall not condense. Since $n_{\text{Pu},v}$ is only dependent on the temperature, the equilibrium problem can be described in terms of the value of $(\text{HX})^2/(\text{H}_2)$ which is necessary in order to maintain a given total fuel concentration, n_2 , at a given temperature.

The equilibrium constant is related to the free energy change of the reaction, Eq. (1), by,

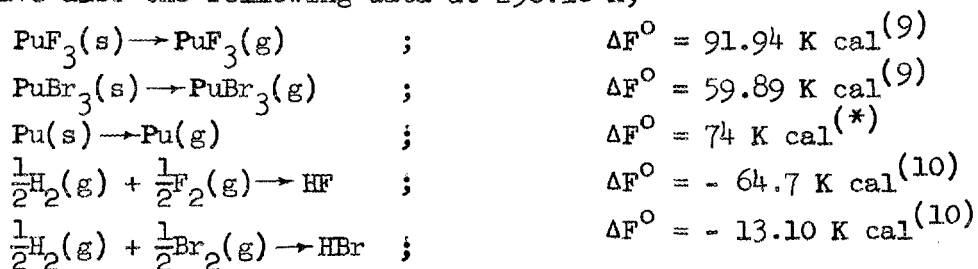
$$\log K_p = -\Delta F^\circ/RT \quad \text{III-(4)}$$

Values of ΔF° have been given at 298.16°K for the reaction,



They are: - 712 K cal for PuF_3 and - 367 K cal for PuBr_3 .⁽⁹⁾

We have also the following data at 298.16°K,



*Estimated from vapor pressure data

Thus, the free energy changes for Eq. (1) are,

$$\begin{aligned} \text{PuF}_3 : \\ \Delta F_{298}^{\circ} = + 712 - 2(91.94) + 2(74) + 6(- 64.7) = 288 \text{ K cal} \end{aligned} \quad \text{III-(5)}$$

$$\begin{aligned} \text{PuBr}_3 : \\ \Delta F_{298}^{\circ} = 367 - 2(59.89) + 2(74) + 6(- 13.10) = 317 \text{ K cal} \end{aligned} \quad \text{III-(6)}$$

At 298^oK, PuBr₃ is evidently somewhat more stable in hydrogen than PuF₃, because the free energy of formation of HBr is so much less than that of HF.

In order to compute the free energy change, ΔF° , at elevated temperatures, it is necessary to estimate the free energy changes of the products and reactants of Eq. (1). The free energies are available for H₂ and HF or HBr. They must be computed for PuF₃(g), PuBr₃(g) and Pu(g).

Calculation of free energies:

Since Pu(g) is monatomic, its free energy can be computed quite readily unless its electronic degrees of freedom are excited. It will be assumed for present purposes that they are not. For the PuF₃ and PuBr₃ a knowledge of the vibrational frequencies of the molecule is needed for computing the free energy. Such information is not available for the PuBr₃, and only rough estimates (from data on PuF₆) are available for PuF₃. Accordingly the following equilibrium estimates will be restricted to the PuF₃ system.

The free energy of a perfect gas with internal degrees of freedom is given by⁽¹¹⁾,

$$F = RT \left\{ \log \left[\frac{h^3}{(2\pi mkT)^{3/2}} \left(\frac{p}{kT} \right) \right] - \log Q_{\text{int}} \right\}, \quad \text{III-(7)}$$

where Q_{int} is the internal partition function, and the other notation is conventional.

In the case of gaseous Pu, without electronic excitation, the free energy is given by the first term of Eq. (7). After substitution of the appropriate values, the expression becomes,

$$F^0/RT = \log(0.0105/T^{5/2}), T = ^\circ K, Pu(g) \quad \text{III-(8)}$$

In the case of PuF_3 it is necessary to evaluate the internal partition function. In the absence of rotational-vibrational interactions and electronic excitation,

$$Q_{\text{int}} = Q_{\text{rot}} Q_{\text{vib}} \quad \text{III-(9)}$$

It will be assumed in evaluating the rotational partition function, Q_{rot} , that the molecule is a symmetrical top, i.e., that the F atoms are arranged with 120 degree separation in a plane. The rotational partition function is then⁽¹¹⁾,

$$Q_{\text{rot}} = \frac{8\pi^2(2\pi kt)^{3/2} I_1 I_2^{1/2}}{6 h^3}, \quad \text{III-(10)}$$

where I_1 is the moment of inertia about an axis perpendicular to the plane of the molecule, and I_2 is the moment of inertia about an axis in the plane. To evaluate Q_{rot} , we need the interatomic distance. Following Hawkins et al⁽¹²⁾, we take this distance as 1.97 \AA . The rotational partition function then becomes,

$$Q_{\text{rot}} = 5.77 T^{3/2}, T = ^\circ K \quad \text{III-(11)}$$

For the purpose of computing the vibrational partition function, the molecule may be replaced by a set of six harmonic oscillators, in which case⁽¹¹⁾,

$$Q_{\text{vib}} = \prod_{i=1}^6 \left[\frac{1}{1 - \exp(-u_i)} \right] \quad \text{III-(12)}$$

where $u_i = h\nu_i/kT$ and ν_i is the frequency of the i^{th} vibrational mode.

There is no precise information on the vibrational frequencies of the PuF_3 molecule; however, the wave numbers⁽¹³⁾ and degeneracies⁽¹⁴⁾ for PuF_6 are as follows:

ω, cm^{-1}	degeneracy
631	1
523	2
202	3
173	3
210	3
615	3

It seems reasonable to assign the higher of these frequencies to "stretching" vibrations, and the lower to "bending" vibrations for the Pu-F bond. Then for the average stretching frequency we get, $[(1)(631) + 2(523) + 3(615)] / 6 = 587 \text{ cm}^{-1}$, and for the bending frequency, $[(3)(202) + (3)(210) + 3(173)] / 9 = 195 \text{ cm}^{-1}$. Since the heat of formation of PuF_3 , per F atom, is considerably higher than that of PuF_6 , it is to be expected that the "stretching" frequencies for PuF_3 will be higher than those for PuF_6 . The heats of formation are $\Delta H_{298} = -125$ and -76 K cal per mole of F.

If the interatomic force law can be approximated by a Morse potential,

$$U(r - r_e) = D_e \left[1 - e^{-\beta(r - r_e)} \right]^2,$$

the frequency of oscillation about the equilibrium point, r_e , is $\nu = (2D_e \beta^2 / m)^{1/2}$, where m is the reduced mass for the mode in question. For lack of information, β and r_e will be assumed to be the same for the Pu-F bonds in PuF_3 and PuF_6 , when

$$\nu_{\text{PuF}_3} = \left(\frac{D_{e, \text{PuF}_3}}{D_{e, \text{PuF}_6}} \right)^{1/2} \nu_{\text{PuF}_6},$$

and if $D_e \propto -\Delta H_{298}$ as given above, then

$$\nu_{\text{PuF}_3} \approx 1.28 \nu_{\text{PuF}_6}.$$

Applying this correction to the "stretching" frequency found for PuF_6 , we have the following frequencies for PuF_3 :

ω, cm^{-1}	degeneracy
751	3
195	3

The vibrational partition function is now,

$$Q_{\text{vib}} = 1 / \left[1 - e^{-u_1} \right]^3 \left[1 - e^{-u_2} \right]^3 \quad \text{III-(13)}$$

where

$$u_1 = 1.08 \times 10^3 / T, \quad T = ^\circ\text{K}$$

$$u_2 = 0.281 \times 10^3 / T, \quad T = ^\circ\text{K}.$$

Substituting Eqs. (11) and (13) into Eq. (7), we find for the PuF_3 ,

$$F^{\circ}/Rt = \log \left\{ \frac{0.00132 \left[1 - e^{-u_1} \right]^3 \left[1 - e^{-u_2} \right]^3}{T^4} \right\}, \quad T = ^\circ\text{K}, \text{PuF}_3(\text{g}) \quad \text{III-(14)}$$

With Eqs. (8) and (14) for the free energies of $\text{Pu}(\text{g})$ and $\text{PuF}_3(\text{g})$, and tabulated values for HF and H_2 , the value of ΔF_T° for Eq. (1) may be computed according to,

$$\begin{aligned} \Delta F_T^{\circ} = & \Delta F_{298}^{\circ} + 2(F_T^{\circ} - F_{298}^{\circ})_{\text{Pu}(\text{g})} + 6(F_T^{\circ} - F_{298}^{\circ})_{\text{HF}} \\ & - 2(F_T^{\circ} - F_{298}^{\circ})_{\text{PuF}_3(\text{g})} - 3(F_T^{\circ} - F_{298}^{\circ})_{\text{H}_2} \end{aligned} \quad \text{III-(15)}$$

The results are shown in Fig. 21, together with $\log K_p$ computed from Eq. (4). It is clear that as the temperature rises the reaction tends more and more to proceed to the right as would be expected. The values of $F_T^{\circ} - F_{298}^{\circ}$ used in the calculation of Fig. 21 are shown in Fig. 22.

UNCLASSIFIED
ORNL-LR-DWG 30581

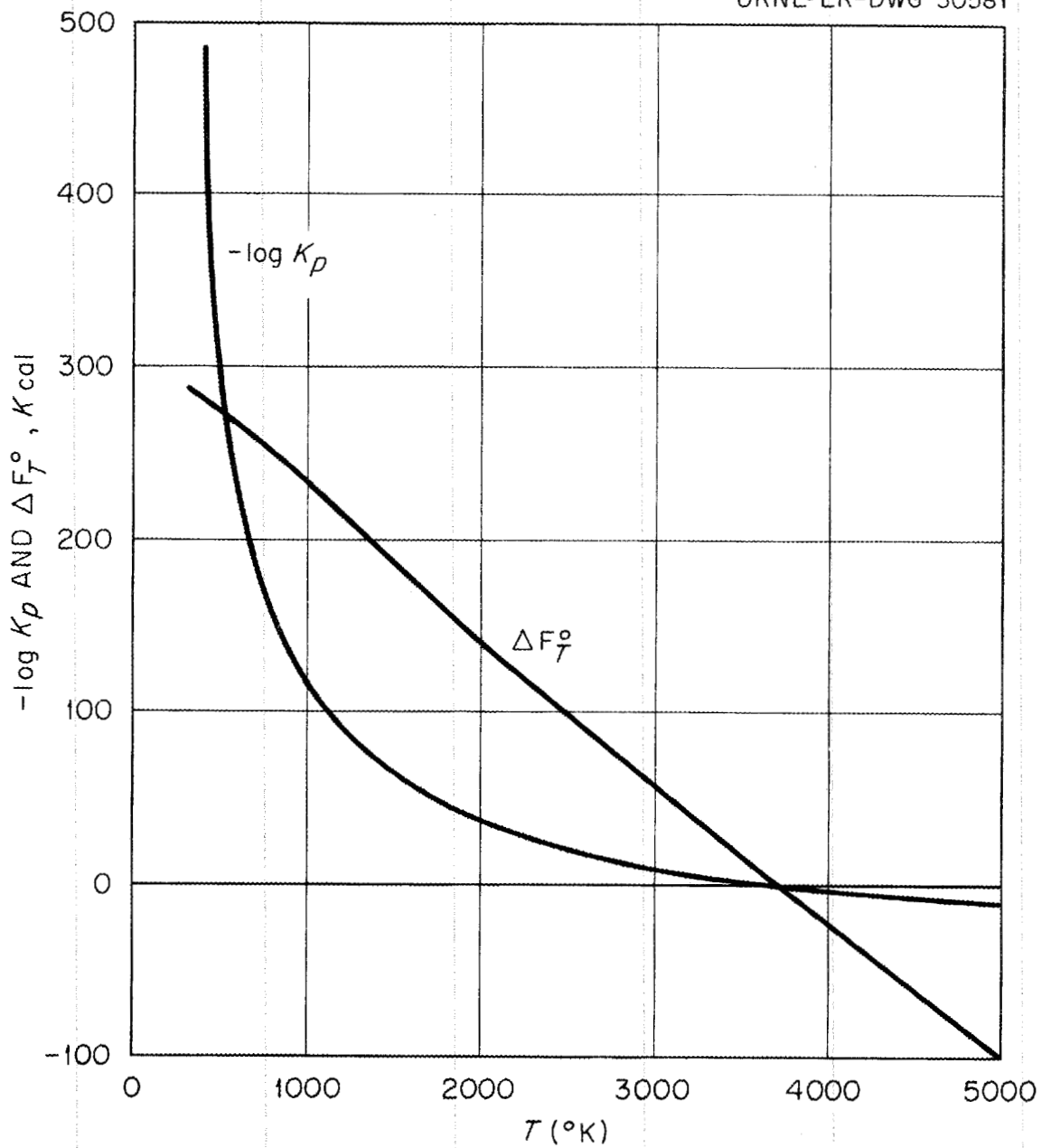


Fig. 21. Free Energy Change and Equilibrium Constant for the Reaction of Gaseous PuF_3 and H_2 to Form Gaseous Pu and HF .

UNCLASSIFIED
ORNL-LR-DWG 30582

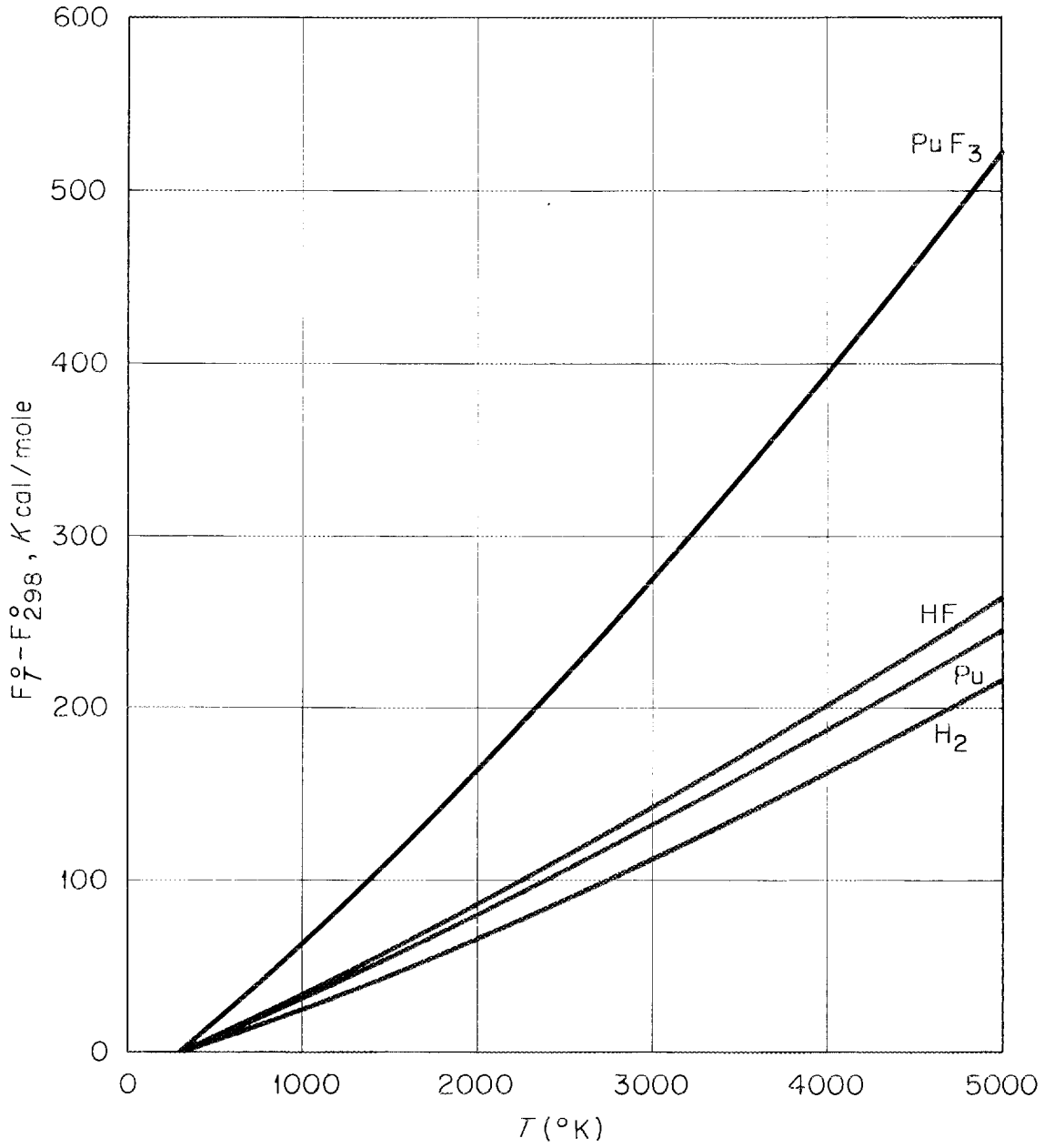


Fig. 22. Free Energy Changes for PuF_3 , Pu , HF , and H_2 .

2. In order to stabilize either PuF_3 or PuBr_3 against reduction by hydrogen at the temperatures of interest, appreciable concentrations of the reduction products (HF or HBr) must be maintained in the vortex tube. The attendant loss in specific impulse, due to dilution of the exhaust gas with HF or HBr, may be more than 20 percent for PuF_3 , if the average fuel concentration is 10^{16} cm^{-3} , and will increase if the fuel concentration is increased.

Requirements imposed by vapor pressure and equilibrium:

The ratio of the square of the partial pressure of HF to the partial pressure of H₂, required to prevent condensation of Pu, may be estimated from the vapor pressure data of Fig. 20 and the values of K_p estimated above. It is clear that Eq. (3) has no meaning if n₂ < n_{Pu,v}, since then all of the fissionable material may exist as gaseous Pu, and no PuF₃ need be stabilized: (HF) is then zero. On the other hand, if n₂ > n_{Pu,v}, some PuF₃ must be held in gaseous form, and Eq. (3) gives the ratio (HF)²/(H₂) required to stabilize this concentration of PuF₃ against reduction. These results are shown in Fig. 23.

Curves of concentration versus temperature are shown for two typical vortex configurations. Each requires a maximum value of log₁₀ [(HF)²/(H₂)] of about - 0.6, hence (HF)²/(H₂) ≥ 0.25. Now if (H₂) is 100 atm, (HF) is 5 atm, and a mole fraction of HF of 0.05 is required to stabilize the PuF₃. The average molecular weight of the propellant is then $\bar{M} = (0.95)(2) + (0.05)(20) = 2.90$. The specific impulse is thus reduced by about 20 percent.

It must be borne in mind in considering the above examples that the influence of the vortex field, in separating products and reactants of the reduction, will tend to increase the required concentrations of HF. Also, higher concentrations will be required if the average fissionable material concentration, \bar{n}_2 , is to be increased beyond 10¹⁸ cm⁻³.

Conclusions:

On the basis of the preceding analysis, the following tentative conclusions seem justified. They should be reviewed if more exact thermochemical data becomes available.

1. To provide the gaseous fuel concentrations necessary for vortex reactors, a polyatomic compound of plutonium is necessary, since metallic plutonium has insufficient volatility. The most promising compounds appear to be PuF₃ and PuBr₃.

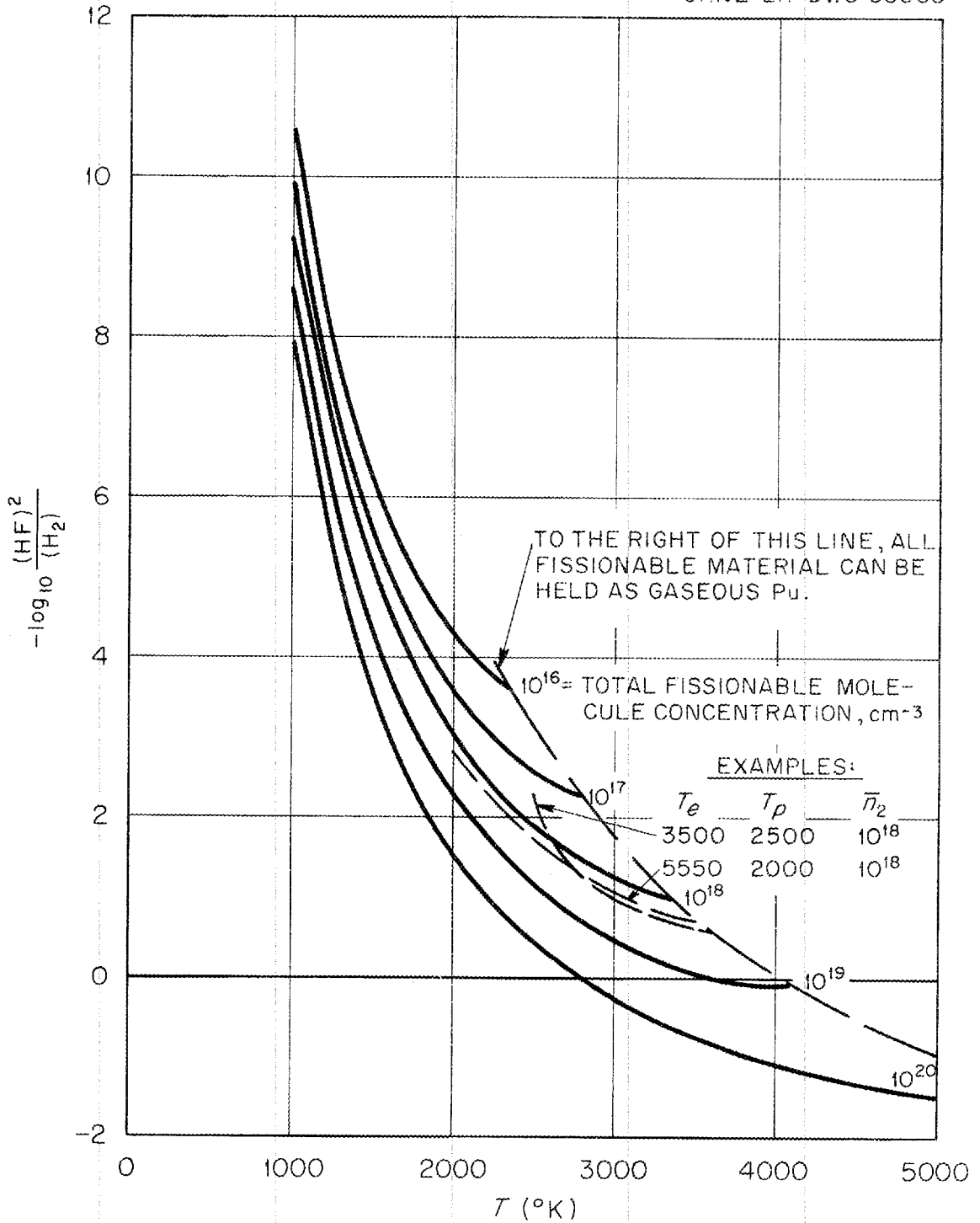


Fig. 23. Concentrations of HF Required to Maintain Given Total Fissionable Material Concentration, as Function of Temperature.

SECTION IV

Fission Product Retention

Introduction:

In five minutes operating time a 300,000 lb thrust vortex reactor with a specific impulse of 1400 will produce one-fifteenth the contamination of a Hiroshima-type bomb, if all of the fission products are released to the atmosphere. It is therefore important to determine to what extent fission fragments produced within the vortex tubes will be contained by the vortex field.

Fission fragments having a range of masses will be produced locally in the vortex tube at a rate proportional to the fissionable material concentration, and will diffuse toward the vortex tube exit under the combined influences of the vortex field and radial flow. The distribution of fission fragments within the tube will start from zero initially and grow to an equilibrium distribution at some later time. After this equilibrium distribution has been attained, the rate of loss of fission fragments will equal the generation rate within the vortex tube. Thus, the rate of loss of fission fragments will increase from zero initially to the maximum possible value when the distribution has attained equilibrium. The objective of the following analysis is to determine the variation of the loss rate with time.

Each fission will be assumed to result in two fission fragments, having half the mass of a fissile atom, deposited as neutral particles at the point of fission. Since the concentration of the fragments will be small compared to that of the propellant and that of the fissionable material, the latter concentrations will not be effected by the fission fragments. Thus, the pressure, the temperature, and the densities of propellant and fissionable material will be those given by the analysis of Ref. 1. The variables describing the behavior of the fission fragments are then reduced to the fission fragment concentration and diffusion velocity.

In the following sections, the differential equations governing these variables will be given, and their solution presented for an example selected from Ref. 1.

Nomenclature:

The principle notation used in the analysis is as follows:

d_{12} \equiv effective hard sphere diameter for collisions between fissionable and propellant molecules.

d_{13} \equiv effective hard sphere diameter for collisions between fission fragments and propellant molecules.

D \equiv diffusion parameter (Eq. (5)).

k \equiv Boltzmann's constant.

m_1 \equiv mass of propellant molecule.

m_2 \equiv mass of fissionable molecule.

m_3 \equiv mean mass of fission fragment.

M_t \equiv tangential Mach number, based on speed of sound in light gas.

\dot{m}_1 \equiv mass flow rate of propellant per unit length of vortex tube.

n_1 \equiv molecular concentration of propellant.

n_2 \equiv molecular concentration of fissionable gas.

n_3 \equiv molecular concentration of fission fragments.

n_0 \equiv total molecular concentration.

p_0 \equiv total pressure.

r \equiv radial coordinate.

T \equiv gas temperature.

u_1 \equiv diffusion velocity of propellant.

u_2 \equiv diffusion velocity of fissionable gas

u_3 \equiv diffusion velocity of fission fragments.

u_0 \equiv mass averaged velocity.

w \equiv ratio of densities of fissionable and propellant gases.

Nomenclature (cont)

- γ = ratio of specific heats for propellant.
 ρ_0 = total density of gas mixture.
 ϕ = neutron track length.

Subscripts:

On independent variable (r or r^*),

c - exit from tube

p - periphery of tube

m - point of maximum w

On dependent variables,

0 - value for gas mixture

1 - value for propellant

2 - value for fissionable gas

3 - value for fission fragments.

Superscripts:

* - quantity divided by its value at point of maximum w .

Differential equations:

If n_3 is the concentration of fission fragments, u_3 their diffusion velocity, u_0 the mass-averaged velocity, r the radial coordinate and S the rate of generation of fission fragments per unit volume, the continuity equation for the fission fragments is,

$$r \frac{\partial n_3}{\partial t} + \frac{\partial}{\partial r} [rn_3(u_0 + u_3)] = rS \quad \text{IV-(1)}$$

By making use of the facts that the fissionable material concentration, n_2 , and the fission fragment concentration are much smaller than the propellant concentration, the equation connecting the diffusion velocities of the fission fragments and propellant may be written as follows, ⁽¹⁵⁾

$$u_3 - u_1 = -D_{13} \frac{n_0}{n_3} \left[\frac{\partial}{\partial r} \left(\frac{n_3}{n_0} \right) + \left(\frac{n_3}{n_0} - \frac{c_3 m_3}{\rho_0} \right) \frac{1}{p_0} \frac{dp_0}{dr} \right]. \quad \text{IV-(2)}$$

Here D_{13} is the binary diffusion coefficient for fission fragments and propellant, n_0 is the total molecular concentration, m_3 is the fission fragment mass, and ρ_0 and p_0 are the total density and pressure. The source of fission fragments, S , is given by

$$S = 2\sigma_f \phi n_2, \quad \text{IV-(3)}$$

where σ_f and ϕ are the fission cross section and neutron flux.

Equations (1), (2) and (3) are sufficient to solve for the concentration, n_3 , if proper boundary conditions are specified. These will be given later. It is convenient to reduce the equations to a dimensionless form before attempting their solution. All of the quantities given by Ref. 1 will be nondimensionalized as they were in Ref. 1, by dividing them by their values at the point in the tube where $w = n_2 m_2 / n_1 m_1$ has its maximum value. These dimensionless quantities are indicated by an asterisk. If u_{0m} and r_m are the mass averaged velocity and radius at the point of maximum w , we may then write Eq. (2) as,

$$\frac{u_3 - u_1}{u_{Om}} = - \frac{D_{13}}{r_m u_{Om}} \left[\frac{1}{n_3} \frac{\partial n_3}{\partial r^*} - \frac{1}{n_1^*} \frac{\partial n_1^*}{\partial r^*} + \left(1 - \frac{m_3/m_1}{1+w} \right) \frac{1}{p_0^*} \frac{dp_0^*}{dr^*} \right]$$

Now u_1/u_{Om} is found from Ref. 1 to be

$$\frac{u_1}{u_{Om}} = u_0^* w \left(\frac{1 - w_c/w}{1 + w_c} \right),$$

where w_c is the value of w at the vortex exit. Also,

$$\frac{1}{n_1^*} \frac{dn_1^*}{dr^*} = \frac{1}{p_0^*} \frac{dp_0^*}{dr^*} - \frac{1}{T^*} \frac{dT^*}{dr^*},$$

and using Eq. (10) of Ref. 1, we find,

$$\frac{u_3}{u_{Om}} = u_0^* w \left(\frac{1 - w_c/w}{1 + w_c} \right) - \frac{D_{13}}{r_m u_{Om}} \left[\frac{1}{n_3} \frac{\partial n_3}{\partial r^*} + \frac{1}{T^*} \frac{dT^*}{dr^*} - \gamma M_{tm}^2 \frac{m_3}{m_1} \frac{1}{r^* 3} T^* \right]. \quad \text{IV-(4)}$$

Here M_{tm} is the tangential Mach number in the vortex at the point of maximum w .

By analogy to Eq. (24) of Ref. 1, we take

$$\frac{D_{13}}{r_m u_{Om}} = - \delta_{m3} \frac{T^* 3/2}{p_0^*},$$

where

$$\delta_{m3} = - \frac{3(2\eta)^{1/2}}{8} \left(\frac{k^{1/2} m_1^{1/2}}{d_{13}^2} \right) \left(1 + \frac{m_1}{m_3} \right)^{1/2} \left(\frac{1 + w_m}{1 + w_c} \right) \frac{T_m}{\mathcal{M}_1}^{1/2}$$

and \mathcal{M}_1 is the mass flow rate of propellant, per unit of tube length.

d_{13} is the effective hard-sphere diameter for collisions between fission

fragments and propellant. Now if \mathcal{D}_{m2} is the quantity defined by Eq. (24) of Ref. 1, then

$$\mathcal{D}_{m3} = \left(\frac{1 + \frac{m_1}{m_3}}{1 + \frac{m_1}{m_2}} \right)^{1/2} \left(\frac{d_{12}}{d_{13}} \right)^2 \mathcal{D}_{m2} ,$$

but from Eq. (34), Ref. 1,

$$\mathcal{D}_{m2} = \frac{(1 - w_c/w_m)(1 + w_m)}{\gamma M_{tm}^2 \left(\frac{m_2}{m_1} - 1 \right) (1 + w_c)} ,$$

and

$$\mathcal{D}_{m3} = \frac{(1 - w_c/w_m)(1 + w_m)}{\gamma M_{tm}^2 \left(\frac{m_2}{m_1} - 1 \right) (1 + w_c)} \left(\frac{1 + \frac{m_1}{m_3}}{1 + \frac{m_1}{m_2}} \right)^{1/2} \left(\frac{d_{12}}{d_{13}} \right)^2 . \quad \text{IV-(5)}$$

The continuity equation, Eq. (2), may also be written in dimensionless form,

$$r^* \frac{\partial n_3}{\partial t} + \frac{u_{Om}}{r_m} \frac{\partial}{\partial r^*} \left[r^* n_3 \left(u_0^* + \frac{u_3}{u_{Om}} \right) \right] = r^* S .$$

Eliminating u_3/u_{Om} from this equation with Eq. (4), we find

$$r^* \frac{\partial n_3}{\partial t} + \frac{u_{Om}}{r_m} \frac{\partial}{\partial r^*} \left[a(r^*) n_3 + b(r^*) \frac{\partial n_3}{\partial r^*} \right] = r^* S ,$$

where

$$a(r^*) = r^* u_0^* \left(\frac{1+w}{1+w_c} \right) + \beta_{m3} r^* \frac{T^{*3/2}}{p_0^*} \left(\frac{1}{T^*} \frac{dT^*}{dr^*} - \gamma M_{tm}^2 \frac{m_3}{m_1} \frac{1}{r^{*3} T^*} \right), \quad \text{IV-(6)}$$

and

$$b(r^*) = \beta_{m3} r^* \frac{T^{*3/2}}{p_0^*}. \quad \text{IV-(7)}$$

Carrying out the indicated differentiation,

$$r^* \frac{\partial n_3}{\partial t} + \frac{u_{0m}}{r_m} b(r^*) \frac{\partial^2 n_3}{\partial r^{*2}} + \frac{u_{0m}}{r_m} \left[a(r^*) + \frac{db(r^*)}{dr^*} \right] \frac{\partial n_3}{\partial r^*} + \frac{u_{0m}}{r_m} \frac{da(r^*)}{dr^*} n_3 = r^* S \quad \text{IV-(8)}$$

Now S is given by Eq. (3). We define a mean lifetime, τ_2 , for a fissionable atom as

$$\tau_2 \equiv \frac{1}{\sigma_f \phi} \quad \text{IV-(9)}$$

and write S as

$$S = \frac{2n_{2m}}{\tau_2} n_2^*.$$

A quantity which is characteristic of the fluid residence time in the tube may be defined as,

$$\tau_1 \equiv \frac{r_m}{u_{0m}}. \quad \text{IV-(10)}$$

We then find that if a new variable, η , is defined as

$$\eta \equiv \frac{n_3}{2n_{2m}} \frac{\tau_2}{\tau_1}, \quad \text{IV-(11)}$$

and a new time variable is defined as

$$\xi \equiv t/\tau_1, \tag{IV-(12)}$$

the differential equation takes the final form,

$$\frac{\partial \eta}{\partial \xi} - f(r^*) \frac{\partial^2 \eta}{\partial r^{*2}} - g(r^*) \frac{\partial \eta}{\partial r^*} - h(r^*) \eta = n_2^* \tag{IV-(13)}$$

where

$$f(r^*) = \frac{b(r^*)}{r^*} = \rho_{m3} \frac{T^{*3/2}}{p_0^*} \tag{IV-(14)}$$

$$g(r^*) = u_0^* \left(\frac{1+w}{1+w_c} \right) + f(r^*) \left[\frac{1}{r^*} + \frac{5}{2} \frac{1}{T^*} \frac{dT^*}{dr^*} - \gamma M_{tm}^2 \left(\frac{m_3}{m_1} + 1 + w \right) \frac{1}{r^* T^*} \right] \tag{IV-(15)}$$

$$h(r^*) = \frac{1}{r^*} \frac{d}{dr^*} [a(r^*)] \tag{IV-(16)}$$

The particular advantage of this form is that all of the coefficients in the equation are of order unity, since all the quantities with asterisks are unity at at least one point in the tube.

Boundary conditions:

The region of interest extends from the tube exit, at r_c^* , to its periphery, at r_p^* . At the periphery, the physical boundary condition is that the mass flow of fission fragments must be zero. This requires that $n_3 m_3 (u_0 + u_3)$ be zero at r_p^* . Since n_3 will in general not be zero at r_p^* , we find from Eqs. (4), (6), and (7)

$$\left. \frac{1}{\eta} \frac{\partial \eta}{\partial r^*} \right|_{r_p^*} = - \frac{a(r_p^*)}{b(r_p^*)} \tag{IV-(17)}$$

At the tube exit, the physical boundary condition is that the gas mixture is rapidly swept from the tube. This is equivalent to saying that at that point u_3 is small compared to u_0 . We therefore put u_3 equal to zero at r_c^* . From Eqs. (4), (6) and (7) again,

$$\left. \frac{1}{\eta} \frac{\partial \eta}{\partial r^*} \right|_{r_c^*} = - \frac{a(r_c^*) - r_c^* u_0^*(r_c^*)}{b(r_c^*)} \quad \text{IV-(18)}$$

With the initial condition that $\eta(r^*, 0) = 0$, the problem is then completely defined.

For complete consistency it is necessary that the value r_c^* , which is taken as the inner boundary of the flow, be the same as that prescribed for a given case in Ref. 1, i.e., the value of r^* at which w is reduced to some specified value, w_c . However, it was shown in Ref. 1 that the value of w_c which was chosen, namely 0.0001, resulted in vortex tubes of very small diameter. It seems likely that an increase in tube diameter from the values computed in Ref. 1, and a corresponding decrease in r_c^* , will be necessary in an actual vortex reactor. Accordingly, in the numerical example which will be given later, the fission product leakage rate will be computed for values of r_c^* less than the value specified by Ref. 1 for $w_c = 0.0001$.

Leakage rate:

In accordance with the above boundary condition at r_c^* , the rate of flow of fission fragments from the tube, per unit of tube length, may be written as,

$$\mathcal{L} = 2\pi r_c n_3(r_c, t) u_0(r_c, t) .$$

In terms of the dimensionless quantities,

$$\mathcal{L}(\xi) = 2 \frac{\tau_1}{\tau_2} \frac{1}{m_2} \frac{w_m}{1 + w_m} \mathcal{N}_1 (1 + w_c) r_c^* u_{0c}^* \eta(r_c^*, \xi) \quad \text{IV-(19)}$$

\mathcal{L} is the loss rate in particles per unit time, and use has been made of the relation

$$M_1(1 + w_c) = 2\pi r_m^2 \rho_{Om} u_{Om} .$$

For large values of ξ , after the equilibrium distribution is attained, we must have

$$\mathcal{L}(\infty) = 2\pi r_p^2 \bar{n}_2 \sigma_f \phi , \tag{IV-20}$$

where \bar{n}_2 is the mean fissionable material concentration in the tube. Combining this with Eq. (19), we find as the asymptotic value of $\eta(r_c^*)$,

$$\eta(r_c^*, \infty) = \frac{r_p^{*2}}{2u_c^* r_c^*} \left(\frac{\bar{w}}{w_m} \right) \left(\frac{\bar{\rho}_1}{\rho_{1p}} \right) \left(\frac{p_{Op}^*}{T_p^*} \right) \tag{IV-21}$$

This relation gives a useful check on the integration of Eq. (13).

Numerical example:

A machine code has been prepared for ORACLE⁽¹⁶⁾, to solve the general linear, time dependent diffusion equation, as typified by Eq. (13). With this code Eq. (13) has been integrated* for an example selected from Ref. 1. Some pertinent data for this example are summarized in Table 1.

TABLE 1 - Data for Numerical Example

M_{tm}	0.7	M_{tp}	0.640
W_m	1.0	$\bar{\rho}_1 / \rho_{1p}$	0.599
$\epsilon_m / \epsilon_m (\text{max.})$	0.338	p_{oc} / p_{op}	0.575
r_p^*	1.24	p_{op}^*	1.224

* The authors are indebted to F. J. Witt for preparing this program [Ref.(16)] and carrying out the machine calculations.

r_c^*	0.725	T_p^*	0.7794
u_{oc}^*	4.113		
T_c/T_p	1.35		
w/w_m	0.361		

The coefficients, $f(r^*)$, $g(r^*)$, and $h(r^*)$ have been computed from Eqs. (14), (15) and (16), and are tabulated in Table 2, along with n_2^* .

Table 2 - Coefficients for Eq. (13)

r^*	$f(r^*)$	$g(r^*)$	$h(r^*)$	$n_2^*(r^*)$
1.245	0.01475	0.6402	0.1925	0.1530
1.205	0.01529	0.6482	0.0505	0.2704
1.165	0.01628	0.6634	-0.2400	0.4609
1.125	0.01779	0.6914	-0.6086	0.6870
1.085	0.01993	0.7347	-1.0219	0.8947
1.045	0.02268	0.8053	-1.3200	1.0195
1.005	0.02594	0.8876	-1.3100	1.0115
0.965	0.02917	0.9798	-0.7305	0.8576
0.925	0.03223	1.0473	0.4222	0.5964
0.885	0.03451	1.0719	2.0747	0.3175
0.845	0.03617	1.0190	3.9093	0.1169
0.805	0.03746	0.8799	5.8188	0.0260
0.765	0.03873	0.6473	7.9166	0.0029
0.725	0.04022	0.2961	10.9466	0.0001
0.685	0.04199	-0.1728	15.3106	0
0.645	0.04424	-1.0213	22.3705	0
0.605	0.4717	-2.2569	34.0764	0
0.565	0.05110	-4.2530	54.6482	0
0.525	0.05656	-7.6432	93.5514	0

In the range of r^* from 1.24 to 0.725 the data were taken directly from the results of Ref. 1. In the range from 0.725 to 0.525, the functions were computed by assuming $w = 0$ and an isentropic expansion. As a first approximation, d_{12}/d_{13} was taken as unity.

The time dependence of η is shown in Fig. (24) for $r_c^* = 0.725$, the value which led to a ratio of heavy gas mass flow to light gas mass flow of 0.0001 in the solution of Ref. 1. The solution grows from a shape similar to that of n_2^* to a shape peaked at a somewhat smaller value of r^* . This inward shift is of course due to the fact that the fission fragments are only one half as heavy as the fissionable molecules.

The variation of $\eta(r_c^*, \xi)$ with ξ is shown in Fig. (25) for this same case. It will be recalled from Eq. (19) that the fission fragment loss rate is proportional to $\eta(r_c^*, \xi)$. The most important fact to be gained from Fig. (25) is that, for $r_c^* = 0.725$, the maximum loss rate is approached in an interval of time corresponding approximately to $\xi = 1$. Recalling the definition of ξ [Eq. (12)], we see that the relaxation time is for this case of the order of the fluid residence time in the vortex tube. It is then clear that for $r_c^* = 0.725$, no appreciable storage of fission fragments occurs. After the first small fraction of a second of operating time they leak out as fast as they are generated.

It is then reasonable to ask what will happen if the inner boundary of the flow is moved inward, to a smaller radius than that required for containment of the fissionable material. The effect of so reducing the core diameter on the asymptotic fission fragment distribution is shown in Fig. (26). The quantity of fission fragments which can be retained increases very rapidly. The steady-state solutions could not be computed for values of r_c^* less than

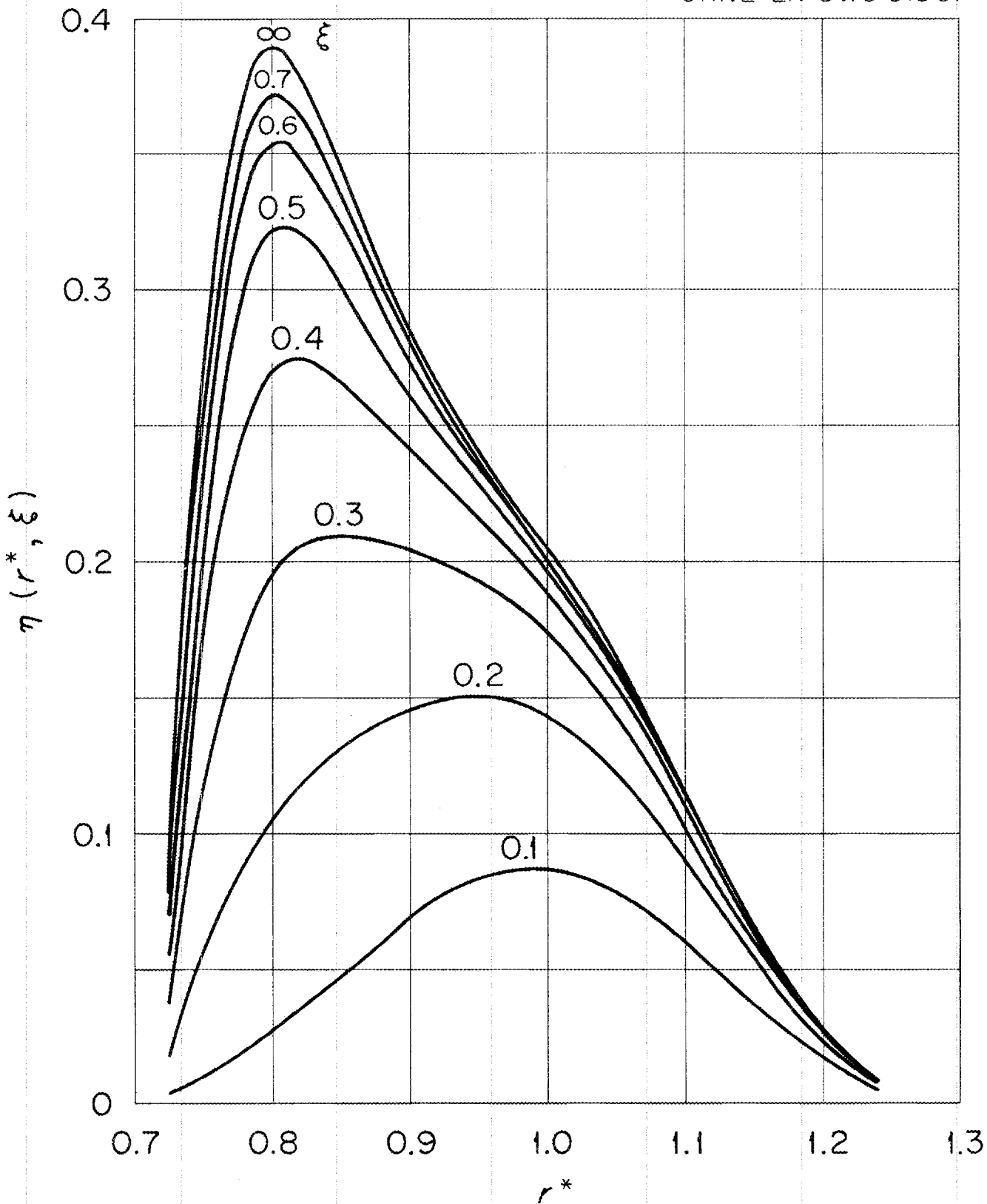


Fig. 24. Development of Dimensionless Fission Fragment Concentration, η , with Dimensionless Time, ξ , for $r_c^* = 0.725$.

UNCLASSIFIED
ORNL-LR-DWG 31862

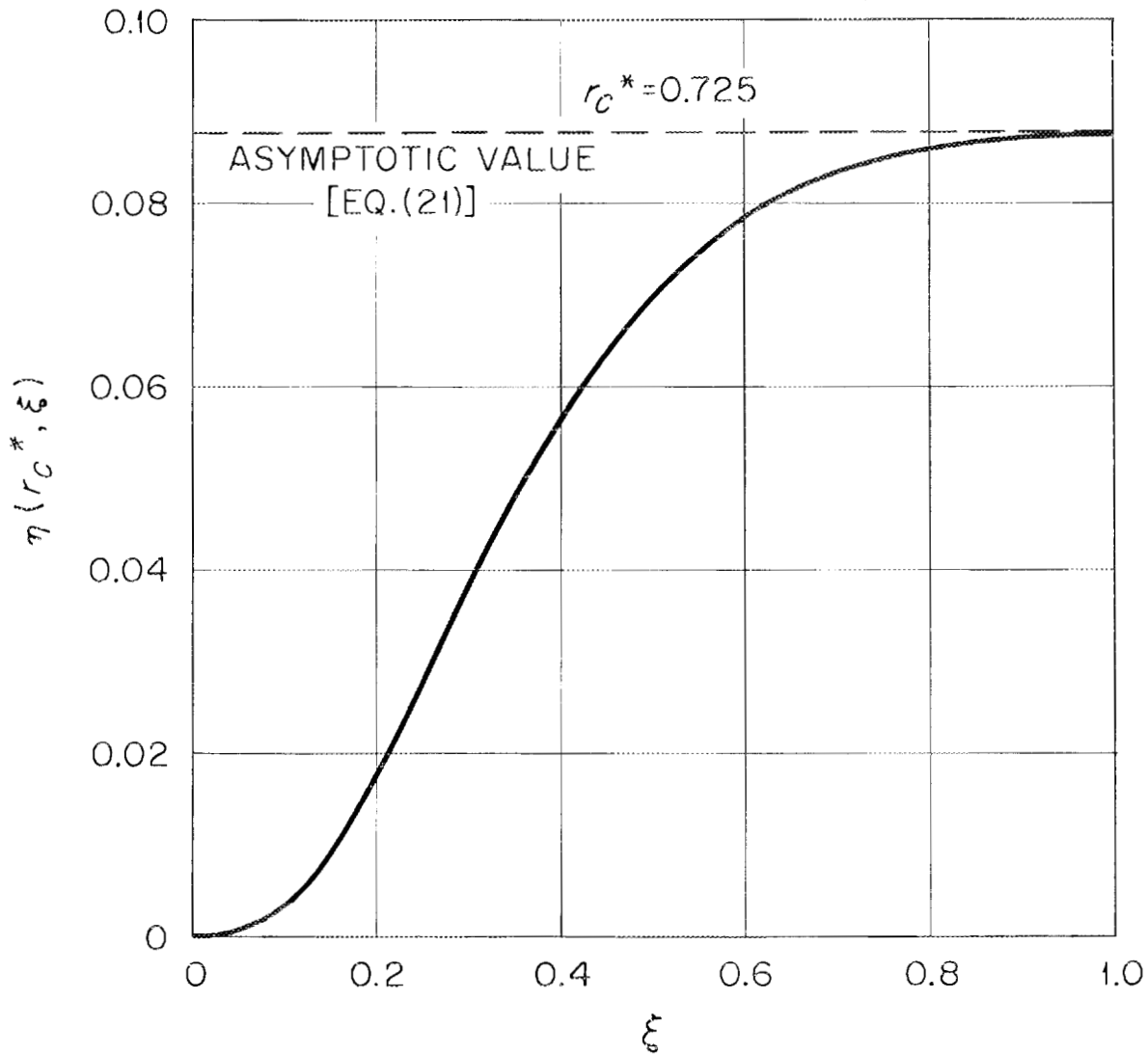


Fig. 25. Variation of Dimensionless Concentration at Inner Boundary [$\eta(r_c^*)$], with Dimensionless Time, ξ , for $r_c^* = 0.725$.

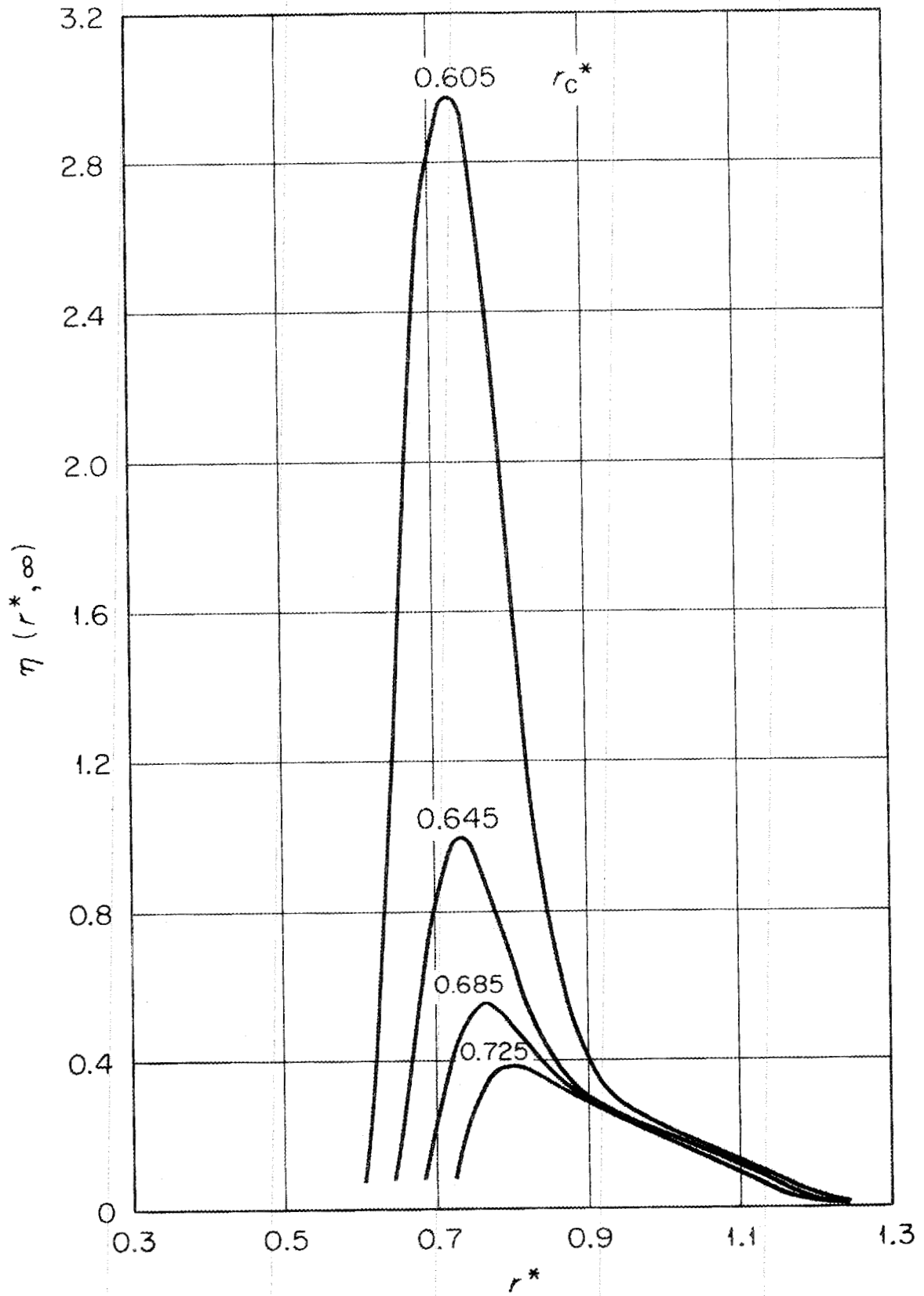


Fig. 26. Dependence of Asymptotic Fission Product Profile on Position of Inner Boundary r_c^* .

0.605 because of machine difficulties, however the transient solution is shown in Fig. (27) for $r_c^* = 0.525$. For this value of r_c^* , the quantity of fission fragments which is stored is more than one hundred times as large as for $r_c^* = 0.725$. As would be expected, the time required for the loss rate to reach its maximum value is also more than one hundred times as large. This is shown in Fig. (28).

For a typical vortex tube as described in Ref. 1, the value of γ_1 , is about 0.1 seconds. Thus, the time required to attain the maximum fission product loss rate, for $r_c^* = 0.525$, is about 10 seconds. While this is still a small time compared to the burning time of a typical large rocket, it seems clear that by reducing r_c^* to a value somewhat smaller than 0.525, the relaxation time could be increased to 100 seconds or longer.

Conclusions:

It is therefore concluded that, by reducing r_c^* to a value approximately one-half of that required for adequate retention of the fissionable material, the rate of loss of fission fragments can be reduced to a small fraction of their rate of generation, at least during the first portion of the rocket's flight.

Because of the complexity of the problem and the large number of independent variables, it does not seem feasible to make this statement more quantitative at the present time. However, the method outlined should be capable of yielding a fairly precise estimate of fission product loss rates for a specific reactor design, should such an estimate be desired.

UNCLASSIFIED
ORNL-LR-DWG 31864

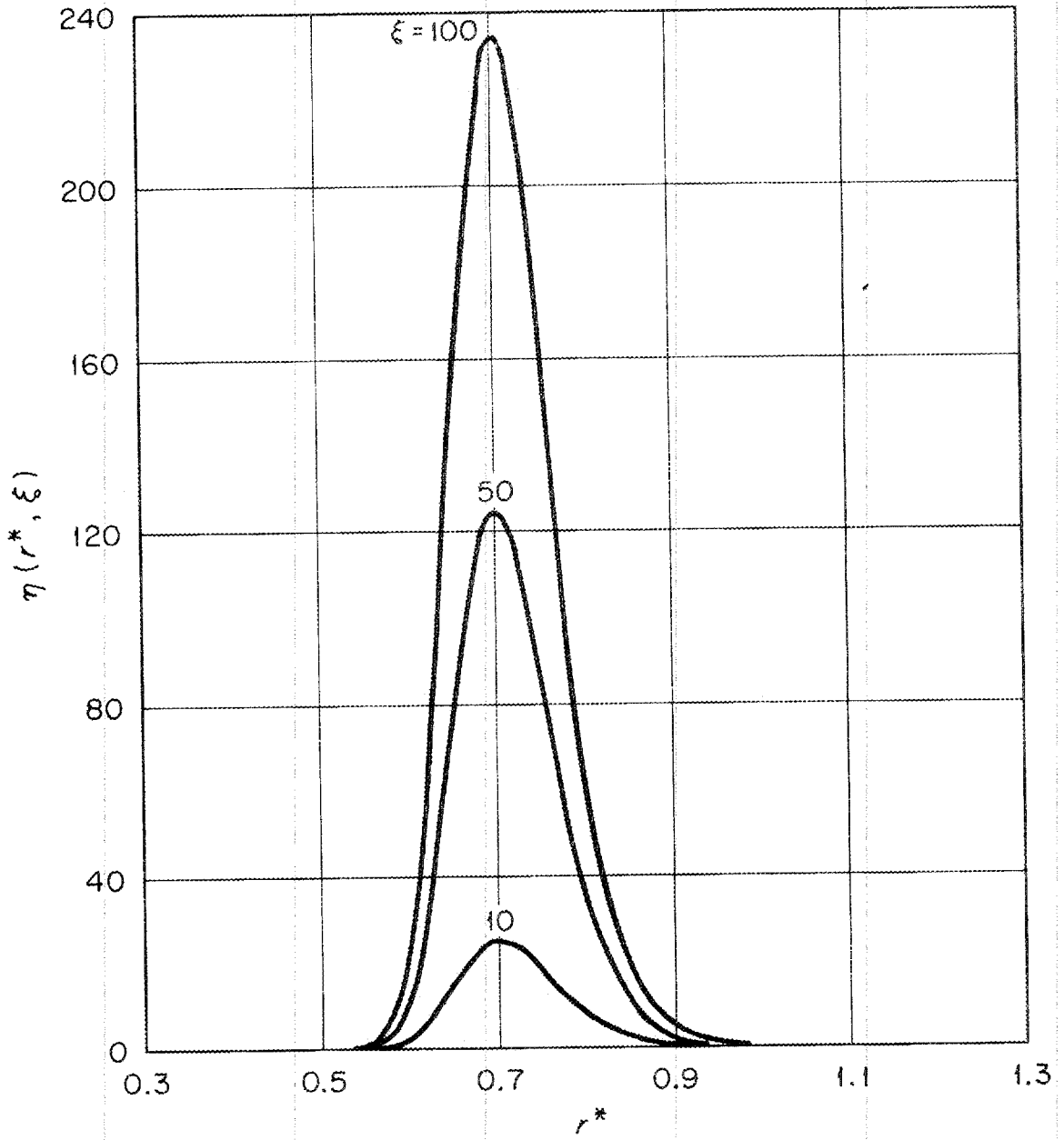


Fig. 27. Development of Dimensionless Fission Fragment Concentration, η , with Dimensionless Time, ξ , for $r_c^* = 0.525$.

UNCLASSIFIED
ORNL-LR-DWG 31865

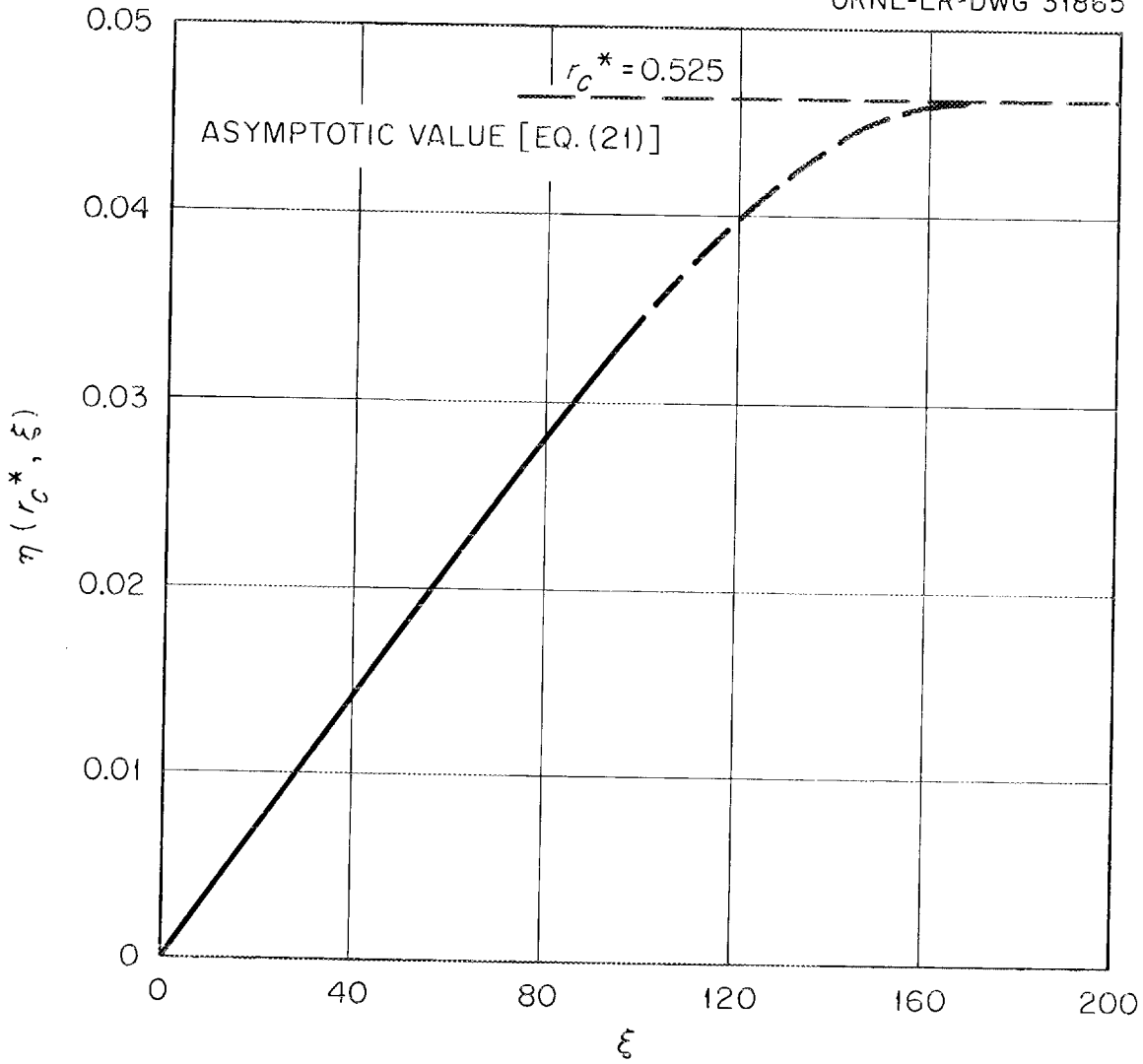


Fig. 28. Variation of Dimensionless Concentration at Inner Boundary [$\eta(r_c^*)$], with Dimensionless Time, ξ , for $r_c^* = 0.525$.

REFERENCES

1. J. L. Kerrebrock and R. V. Meghreblian, An Analysis of Vortex Tubes for Combined Gas-Phase Fission-Heating and Separation of the Fissionable Material, ORNL CF 57-11-3, Rev. 1, April 11, 1958.
2. Pai, Viscous Flow Theory, p. 346, D. Van Nostrand, 1956.
3. R. R. Bate, L. T. Einstein and W. E. Kinney, Description and Operating Manual for the Three Group, Three Region Reactor Code for ORACLE, ORNL CF 55-1-76, January 13, 1955.
4. R. N. R. Mulford and G. E. Sturdy, "Dissociation Pressures for PuH_2 ", J. Am. Chem. Soc., 77, p. 3449 (1955).
5. S. Fried and N. R. Davidson, "Studies in the Dry Chemistry of Plutonium Fluorides", N.N.E.S. Div. IV, 14B, p. 784, McGraw-Hill Book Co.
6. T. E. Phipps, G. W. Sears, R. L. Seifert and O. C. Simpson, "The Vapor Pressure of Plutonium Halides", N.N.E.S. Div. IV, 14B, p. 682, McGraw-Hill Book Co.
7. T. E. Phipps, G. W. Sears and O. C. Simpson, "The Volatility of Plutonium Dioxide", N.N.E.S. Div. IV, 14B, p. 704, McGraw-Hill Book Co.
8. Reactor Handbook, 3, p. 237.
9. L. Brewer, L. Bromley, P. W. Gilles and N. L. Lofgren, "The Thermodynamic Properties and Equilibria at High Temperatures of the Compounds of Plutonium", N.N.E.S. Div. IV, 14B, p. 861, McGraw-Hill Book Co.
10. F. D. Rossini, D. D. Wagman, W. H. Evans, S. Levine and I. Jaffe, Selected Values of Chemical Thermodynamic Properties, National Bureau of Standards Circular 500.

11. R. Fowler and E. A. Guggenheim, Statistical Thermodynamics, Cambridge University Press.
12. N. J. Hawkins, H. C. Mattraw and W. W. Sabol, Infrared Spectrum and Thermodynamic Properties of PuF₆, KAPL-1007, May 24, 1954.
13. John G. Malm and Bernard Weinstock, Argonne Plutonium Hexafluoride Program, ANL-5366 (Secret).
14. J. J. Katz and E. Rabinowitch, "The Chemistry of Uranium", N.N.E.S. Div. VIII, 5, p. 436.
15. F. D. Rossini, The Thermodynamics and Physics of Matter, Princeton University Press, p. 345.
16. F. Joel Witt, "SOL: An Oracle Code for the Solution of Certain Second Order Linear Partial Differential Equations", ORNL Report Number 2585.

LIST OF FIGURES

- (1) Withdrawal of fluid through porous wall.
- (2) Variation of effectiveness of vortex formation, $v_{\theta}(1)/v_j$, with bleed to radial mass flow ratio, M_0/M_1 , and dimensionless tube radius, r_w^* .
- (3) Comparison of vortex tube shear layer velocity profile with Blasius and asymptotic flat plate suction profiles.
- (4) Variation of ratio of shear layer displacement thickness to tube radius, δ^*/r_w , with bleed mass flow rate and dimensionless tube radius.
- (5) Model used for calculation of effect of wall bleed on vortex diffusion.
- (6) Schematic of gas-turbine driven recirculation system.
- (7) Permissible mass flow ratios for gas-turbine recirculation system, as function of compressor pressure ratio and total pressure loss ratio.
- (8) Variation of maximum dimensionless heat exchanger enthalpy rise with turbine outlet temperature, for hydrogen.
- (9) Vortex tube temperature ratios required by gas-turbine recirculation systems.
- (10) Schematic of propellant-turbine driven recirculation system.
- (11) Permissible mass flow ratios for propellant-turbine recirculation system, as function of ratio of turbine and heat exchanger enthalpy changes and total pressure loss ratio.
- (12) Vortex tube temperature ratios required by propellant-turbine recirculation system.
- (13) Variation of macroscopic fission cross section with product of vortex outlet pressure and maximum value of ratio of fuel density to propellant density, for typical vortex reactors.
- (14) Variation of infinite medium multiplication constant with macroscopic fission cross section for typical vortex reactors.
- (15) Variation of reactor (core plus reflector) weight with reflector thickness for typical graphite and beryllium moderated reactors.

- (16) Variation of core radius with reflector thickness for typical reactors.
- (17) Variation of critical mass with macroscopic fission cross section for minimum weight reactors.
- (18) Variation of reactor (core plus reflector) weight with moderator void fraction for typical reactors.
- (19) Variation of core radius with moderator void fraction for typical reactors.
- (20) Vapor pressure limited concentrations for possible fuel carriers.
- (21) Free energy change and equilibrium constant for the reaction of gaseous PuF_3 and H_2 to form gaseous Pu and HF.
- (22) Free energy changes for PuF_3 , Pu, HF, and H_2 .
- (23) Concentrations of HF required to maintain given total fissionable material concentration, as function of temperature.
- (24) Development of dimensionless fission fragment concentration, η , with dimensionless time, ξ , for $r_c^* = 0.725$.
- (25) Variation of dimensionless concentration at inner boundary $[\eta(r_c^*)]$, with dimensionless time, ξ , for $r_c^* = 0.725$.
- (26) Dependence of asymptotic fission product profile on position of inner boundary, r_c^* .
- (27) Development of dimensionless fission fragment concentration, η , with dimensionless time, ξ , for $r_c^* = 0.525$.
- (28) Variation of dimensionless concentration at inner boundary $[\eta(r_c^*)]$, with dimensionless time, ξ , for $r_c^* = 0.525$.